

# Dissociating the contributions of sensorimotor striatum to automatic and visually guided motor sequences

Received: 13 June 2022

Kevin G. C. Mizes<sup>1,2</sup>, Jack Lindsey<sup>3</sup>, G. Sean Escola<sup>1,3,4</sup> & Bence P. Ölveczky<sup>1,2</sup>  

Accepted: 14 August 2023

Published online: 4 September 2023

 Check for updates

The ability to sequence movements in response to new task demands enables rich and adaptive behavior. However, such flexibility is computationally costly and can result in halting performances. Practicing the same motor sequence repeatedly can render its execution precise, fast and effortless, that is, ‘automatic’. The basal ganglia are thought to underlie both types of sequence execution, yet whether and how their contributions differ is unclear. We parse this in rats trained to perform the same motor sequence instructed by cues and in a self-initiated overtrained, or ‘automatic,’ condition. Neural recordings in the sensorimotor striatum revealed a kinematic code independent of the execution mode. Although lesions reduced the movement speed and affected detailed kinematics similarly, they disrupted high-level sequence structure for automatic, but not visually guided, behaviors. These results suggest that the basal ganglia are essential for ‘automatic’ motor skills that are defined in terms of continuous kinematics, but can be dispensable for discrete motor sequences guided by sensory cues.

Our brain’s capacity to organize movements and actions in response to new challenges allows us to imitate trendy dance moves or play Chopin etudes from sheet music. Assembling motor sequences in such flexible and deliberate ways can be mentally taxing and computationally costly, resulting in slow<sup>1</sup> and error-prone performances subject to cognitive interference<sup>2</sup>. However, executing the same motor sequence, such as typing a password or playing a favorite piano sonata, repeatedly and consistently, can turn it into a continuous task-specific movement pattern that is fluid, fast<sup>3–5</sup>, precise<sup>6</sup>, efficient<sup>7</sup> and less cognitively demanding<sup>2,8</sup>, in a word, ‘automatic’<sup>5,9,10</sup>. Thus, the very same motor sequence can be executed in qualitatively and subjectively distinct ways<sup>1,9–11</sup>.

Given that the specification of the same motor sequence can differ so markedly (Fig. 1), the underlying neural circuits are thought to differ as well<sup>5,8,12–14</sup>. For example, a discrete motor sequence informed by external sensory cues will engage a serial action-selection process, while single overtrained, or ‘automatic,’ motor sequences can, by virtue of

being the same every time, be specified in terms of continuous low-level motor commands and sensorimotor policies (Fig. 1c)<sup>15–18</sup>. Indeed, our colloquial reference to automatic behaviors being stored in ‘muscle memory’ reflects a subjective sense that they are, in comparison to sensory-guided motor sequences, less reliant on higher-order cognitive processes and produced by circuits closer to the motor periphery<sup>5,11,12,19</sup>.

Besides being instructed by sensory cues or automatically expressed, motor sequences can also be informed by working memory (Fig. 1b), as is the case when we try to imitate our piano teacher or reproduce our own improvisations from a few moments ago. The generation of such motor sequences is akin to sensory-guided ones in that they too demand considerable mental effort<sup>20</sup> and are defined by (remembered) sensory experiences. Given these shared qualities, we refer to the sensory-guided and working memory-guided sequences as ‘flexible’<sup>13,21</sup> to distinguish them from rote and inflexible automatic motor sequences<sup>1,10</sup>. However, working memory-guided motor

<sup>1</sup>Program in Biophysics, Harvard University, Cambridge, MA, USA. <sup>2</sup>Department of Organismic and Evolutionary Biology and Center for Brain Science, Harvard University, Cambridge, MA, USA. <sup>3</sup>Zuckerman Mind Brain and Behavior Institute, Columbia University, New York City, NY, USA. <sup>4</sup>Department of Psychiatry, Columbia University, New York City, NY, USA.  e-mail: [olveczky@fas.harvard.edu](mailto:olveczky@fas.harvard.edu)

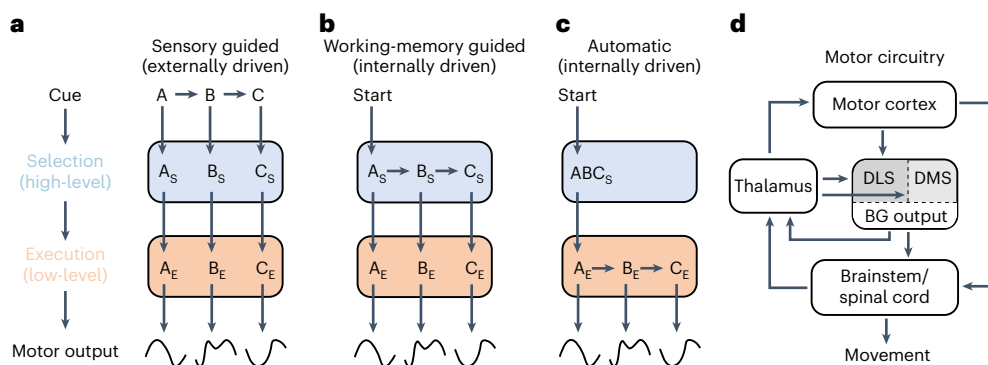


**Fig. 1 | Conceptual schematic showing differences in how a motor sequence can be specified and produced.** **a–c**, Motor control is thought to be hierarchical. To perform a new discrete motor sequence (A-B-C), high-level circuits select and order the requisite motor elements (that is, select A, then B, then C), while low-level circuits implement the detailed control of the movements. The sensory-guided (a) and working memory-guided (b) sequences likely engage higher-order selection-level processes, whereas automatic sequences (c) can become

consolidated and fully specified in low-level execution circuits<sup>5,11,25</sup>. Schematic adapted from refs. 13,25. **d**, Simplified schematic of motor circuits discussed in this study. The basal ganglia (BG) are the nexus of several intersecting motor pathways, allowing them to affect motor implementation by modulating both brainstem and motor cortical dynamics. Omitted, for clarity, are somatosensory and prefrontal projections, cerebellar inputs and dopaminergic midbrain projections.

sequences are also similar to automatic ones in that their progression is informed by internal neural processes. Hence, these two modes of sequence execution, automatic and working memory-guided, are sometimes collectively referred to as ‘internally’ generated, to distinguish them from ‘externally’ cued ones<sup>14,22,23</sup>.

Yet the degree to which the distinctions between ‘flexible’ versus ‘automatic’ and ‘externally’ versus ‘internally’ generated motor sequences map onto specific neural circuits and mechanisms is unclear<sup>13,24,25</sup>. Here we set out to probe how the neural implementations of automatic, visually guided and working memory-guided sequences differ, focusing on the sensorimotor and associative arms of the basal ganglia (BG). Although these pathways have been implicated in various aspects of motor sequence learning and execution<sup>19,26–29</sup>, their specific contribution to sensory-guided, working memory-guided and automatic behaviors has yet to be fully understood<sup>12,14,24,25,30</sup>.

To get at the distinction in how the BG contribute to the different types of motor sequences, we developed a paradigm for rats in which they are trained to perform the very same motor sequence under the three conditions discussed above (Fig. 1). We viewed BG function through the lens of the dorsal striatum, the input zone to the sensorimotor and associative arms of the BG. Surprisingly, neural recordings in sensorimotor striatum (dorsolateral striatum (DLS) in rodents)—a region implicated in behavioral automaticity<sup>5,31</sup>—revealed no meaningful difference across task conditions, with neurons representing low-level kinematic features in all cases. The neural population showed no selectivity for higher-level attributes of the behavior, such as the order or sequential context of a given movement.

Lesions to the DLS, however, revealed a stark contrast across task conditions, with sequence organization being essentially lost for automatic and working memory-guided sequences, but largely preserved for sequences informed by visual cues. Additionally, the movements across all three conditions were slower and more variable postlesion, resembling the animal’s behavior early in learning, a finding consistent with a general role for the BG in specifying the detailed kinematics, including the vigor<sup>15,23</sup>, of learned movements.

## Results

### A discrete sequence production task for rats

To directly compare the neural substrates of visually guided, working memory-guided and automatic motor sequences, we designed, based on similar paradigms in humans and nonhuman primates (NHPs)<sup>14,30,32</sup>, a discrete sequence production task in which rats execute the same

motor sequence in the three different conditions. To distinguish motor automaticity from habit formation<sup>5,33,34</sup>, two independent processes that may involve some of the same neural substrates<sup>5,34</sup>, we wanted our rats to achieve automaticity on a motor sequence without developing it into a habit. Because habits tend to form when the correlation between actions and outcomes is weak or variable<sup>35,36</sup>, if the reward is delayed<sup>37</sup>, or, further, if the reward is appetitive or addictive<sup>38,39</sup>, our paradigm directly linked behavioral variants to a water reward in a training process that resulted in highly overtrained and automatic behaviors expressed in goal-directed ways (Extended Data Fig. 1).

To facilitate comparisons to other motor-related studies in rodents, including our own<sup>15,16</sup>, which probe forelimb<sup>26,29,40–42</sup> and whole-body orienting<sup>43,44</sup> movements, we opted for a ‘piano-playing’ task, in which rats are rewarded for performing sequences of three keypresses on a three-key ‘piano’ in a prescribed order, alternating between forelimb lever presses and orienting movements (12 possible sequences; see Fig. 2a and Supplementary Video 1).

Rats were initially trained to press a single lever for a water reward and then to associate a visual cue above each lever with pressing that lever (Methods). After acquiring the cue-action association for each of the levers ( $5,164 \pm 948$  trials; mean  $\pm$  s.e.m.), rats transitioned from single presses to two- and, ultimately, three-element sequences. In ‘flexible’ training sessions, the rewarded keypress sequence was either signaled directly and sequentially by visual cues (CUE) or had to be remembered from the instructed sequence of previous trials (WM; Methods). This trial design, adopted from studies in NHPs<sup>22</sup>, allowed us to compare performance and neural dynamics for sequences guided by visual cues and internally generated from working memory<sup>14,45</sup>. Blocks of CUE and WM trials were interleaved, and, in each, one of the 12 possible sequences was randomly selected and rewarded (Fig. 2b).

In separate ‘automatic’ sessions (Methods), animals were trained to produce the very same predetermined keypress sequence—randomly chosen for each rat from the 12 possible sequences—for the duration of the months-long experiment (automatic condition, AUTO). Because this automatic sequence is one of the 12 sequences rewarded in the flexible sessions, we could compare the same motor sequence across the three distinct task conditions.

### Rats master the ‘piano-playing’ task

Rats learned to produce the prescribed sequences under all three conditions (CUE, WM and AUTO; Fig. 2c,d). We deemed rats to be ‘experts’ when both their success rates and trial times were reliably within 0.5%

of asymptotic performance values (Methods), which happened after  $17,623 \pm 7,616$  trials ( $75 \pm 23$  d) in the CUE task,  $11,330 \pm 5,278$  trials ( $88 \pm 30$  d) in the WM task and  $14,061 \pm 7,082$  ( $72 \pm 21$  d) trials in the AUTO task.

The success rate of expert rats was, on an average,  $60.19\% \pm 10.73\%$  (CUE),  $44.29\% \pm 15.45\%$  (WM) and  $79.57 \pm 11.84\%$  (AUTO). This success rate is substantially higher than chance performance, which would be  $8.33\%$  considering only the 12 prescribed sequences, or  $3.7\%$  considering all possible three-element keypress sequences. As is expected from similar learning paradigms in humans and NHPs<sup>3,4,14</sup>, the mean and variability of the trial times decreased with learning (Fig. 2e,f), while the stereotypy of the associated movement patterns increased across all three task conditions as did the smoothness and efficiency of the movement trajectories (Fig. 2g; Methods)<sup>7,46</sup>.

### Kinematic similarities across task conditions and movement elements

Distinguishing the neural circuit implementation of the different forms of motor sequence execution requires dissociating differences in task conditions from differences in movement kinematics. To compare kinematics for the same motor sequence across tasks (that is, CUE, WM or AUTO), we tracked the rat's dominant forelimb (that is, the one pressing the lever) and nose from videos recorded from the sides and top (Fig. 2g, Supplementary Video 1 and Extended Data Fig. 2a)<sup>47,48</sup>. Comparing trials of similar duration across the tasks revealed very similar forelimb and nose trajectories (Fig. 2h and Extended Data Fig. 2b,c). Similarity in kinematics is important because it allows us to interpret any potential differences in neural activity and sensitivity to neural circuit manipulations as being due to differences in task condition (AUTO, WM and CUE) rather than low-level aspects of motor implementation.

### Single overtrained motor sequences show the signatures of automaticity

In humans, motor automaticity is distinguished by improved performance, increased movement speed and less variable execution times<sup>1,5,9</sup>. While we found that the kinematics for the same motor sequence across session types was overall similar (Fig. 2e,f and Supplementary Video 1), we parsed these metrics to assess whether automaticity had been established in AUTO sessions (Fig. 3a–d).

Consistent with signatures of automaticity, we found that trials in AUTO sessions were indeed more successful, faster and less variable than when performing the same sequence in flexible sessions (Fig. 3a,c). We also found that the entropy, or randomness, of erroneous sequences was much lower in the AUTO sessions than in either of the flexible sessions (CUE and WM; Fig. 3d), consistent with the idea that errors in automatic sequence execution are more systematic or less variable<sup>49</sup>.

Furthermore, if automatic motor sequences are consolidated and defined in terms of continuous low-level motor commands<sup>15,42,50,51</sup>, and not as serial discrete action selection, unsuccessful trials in AUTO sessions should be dominated by errors relating to variability in movement kinematics (for example, a forelimb swipe at the 'correct' lever

that misses the target), as opposed to errors in higher-level sequencing (Supplementary Video 2). In support of this, failures in AUTO trials were mostly due to rats swiping at but missing the 'correct' lever or failing to depress it beyond the threshold for detection (approximately  $63.81\% \pm 19.56\%$  of all AUTO errors were of this type; Fig. 3e). This was in contrast to flexible sessions, in which unsuccessful attempts were dominated by true sequence errors, where rats orient toward and press the 'wrong' lever (only  $17.6\% \pm 18.25\%$  of CUE and  $29.62\% \pm 19.02\%$  of WM errors were motor errors). Interestingly, potential sequence errors in the AUTO sessions were twice as likely to come after trials with motor execution errors compared to correct trials (Fig. 3f; Methods), consistent with a drop in reward triggering increased motor exploration<sup>49</sup>.

Similar to studies in humans and NHPs<sup>23,52</sup>, rats were also more likely to execute the automatic sequence in flexible sessions compared to chance ( $12.35\% \pm 4.43\%$  in CUE,  $14.99\% \pm 4.85\%$  in WM, where chance is  $8.3\%$ ; Fig. 3g).

In aggregate, these differences in the quality of motor sequence execution and the error modes across the distinct session types are consistent with studies comparing sensory cued and automatic motor sequences in humans<sup>3,4,10</sup> and indicate that automaticity of the over-trained motor sequence, as commonly defined in the literature, had been achieved.

### DLS represents motor sequences similarly across task conditions

We designed our behavioral paradigm to directly probe whether and how the neural implementations of different types of motor sequences differ at the level of the striatum (Fig. 1). To directly and effectively probe this, we implanted 64-channel tetrode drives targeting the DLS in expert rats ( $n = 4$ ; Extended Data Fig. 3a) and compared the activity of the same neurons for the same motor sequence in AUTO, CUE and WM trials. We recorded neural activity continuously over several weeks, comparing units recorded for at least five successful trials in each task condition (CUE, WM and AUTO) for the same motor sequence (in total,  $n = 579$  neurons selected from 2,468 total; Methods).

The comparisons across task conditions (Fig. 4a) were striking for the lack of any qualitative difference—task-related activity patterns of DLS neurons for the same motor sequence were highly correlated across all trial types (CUE, WM and AUTO; Fig. 3a,b,d) with no significant difference in either the average firing rates or peak z-scored activity (Fig. 4c). We found a similar result when splitting the population into putative medium spiny neurons (MSNs) and fast-spiking interneurons (FSIs; Extended Data Fig. 4). Thus, the neural recordings, on their own, did not suggest a meaningful difference in how the BG are engaged in sensory-guided, working memory-guided and automatic motor execution despite prior suggestions to the contrary<sup>12,53–55</sup>.

### The DLS does not encode high-level aspects of the sequence

We next analyzed neural activity patterns in DLS for clues about the general contributions it makes to motor sequence execution, focusing first on its putative role in action selection. Prior studies

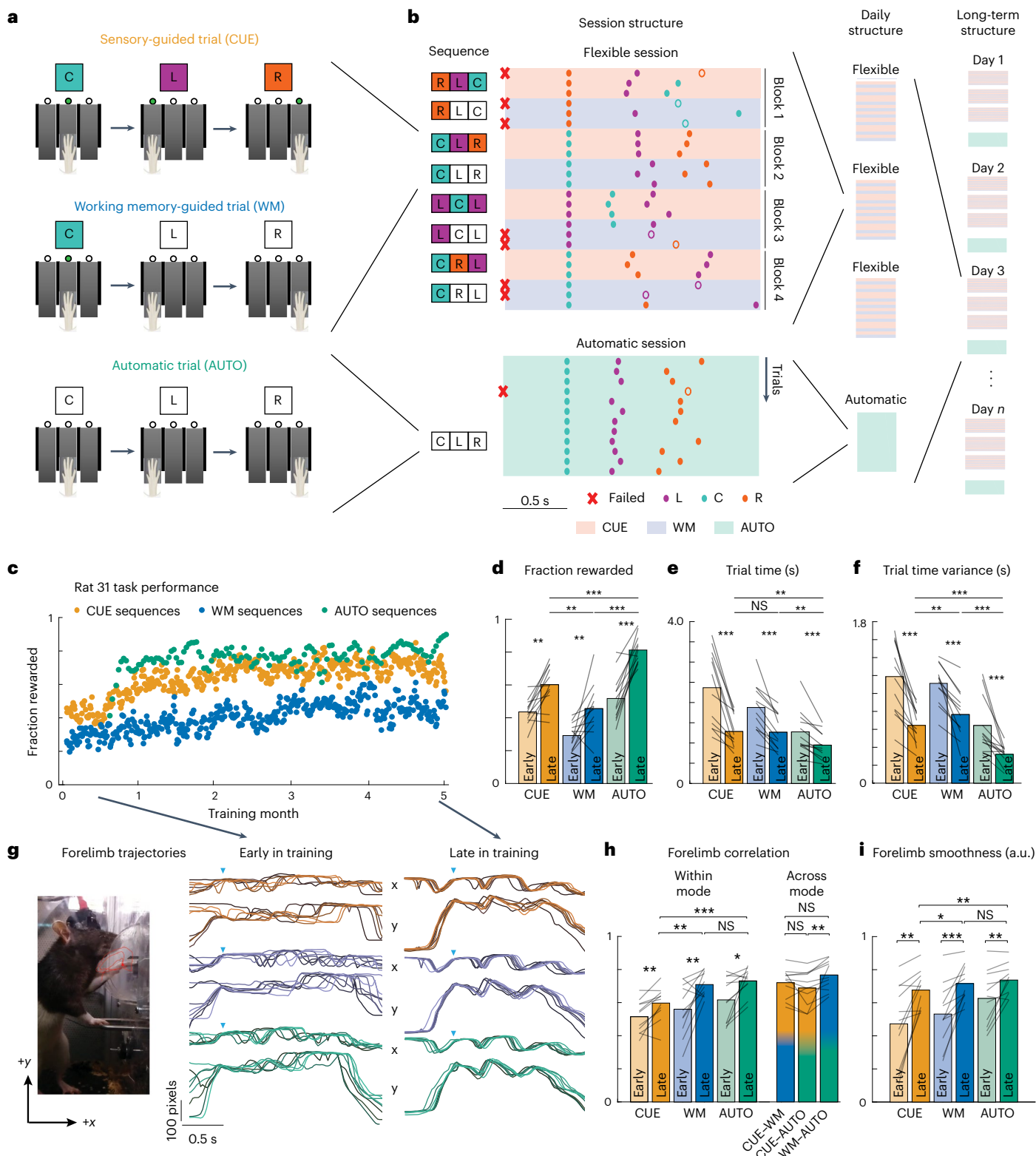
**Fig. 2 | Paradigm for training rats to produce visually guided, working memory-guided and automatic motor sequences. a**, Rats learn to generate three-element lever-press sequences that, in 'flexible' training sessions, are either visually cued (CUE) or generated from working memory by repeating the sequence from the preceding cued trial (WM). In a separate 'automatic' session without any cues, the same sequence is rewarded each day. The automatic (AUTO) sequence is chosen randomly for each rat and fixed for the duration of the experiment. **b**, Performance of an example rat in a flexible (top) and automatic session (bottom). In flexible sessions, sequences are randomly chosen, from 12 possible sequences, and change every block. **c**, Fraction of rewarded trials per session for the three task conditions (orange, CUE; blue, WM; green, AUTO) for one animal over several months of training. **d–f**, Performance metrics improve from early (light shade) to late (dark shade) in learning across

all three task conditions ( $n = 12$  rats). Fraction of rewarded trials (d), trial time (e) and variance in trial time (f). **g**, Vertical (y) and horizontal (x) components of forelimb trajectories, aligned to the first lever press, for eight example trials from early and late in learning, as captured from a side camera. Examples are selected from trials with similar duration. **h**, Trial-to-trial correlation of the active forelimb trajectory within a given task condition from early and late in training ( $n = 11$  of 12 rats were tracked in early learning), and correlation of the kinematics across the three task conditions, late in training. **i**, The smoothness of the movement kinematics, as measured through the inverse of the spectral arc length<sup>46</sup> (Methods), increases over learning ( $n = 11$  of 12 rats tracked in early learning). Values closer to 1 indicate smoother movements. For all panels, \* $P < 0.05$ , \*\* $P < 0.01$ , \*\*\* $P < 0.001$ , two-sided Wilcoxon signed-rank test.

supporting such a function have interpreted elevated average DLS activity at the boundaries of ‘chunked’ actions<sup>41,56,57</sup> as an indication that the BG help bias their initiation and/or termination by facilitating and/or inhibiting downstream control circuits. To test for this, we examined the firing rate modulation over the length of the whole sequence (Fig. 4e; Methods). We found no evidence for population activity in the DLS preferentially marking the start and/or stop of automatic sequences; neither did it consistently mark the

boundaries between behavioral elements (lever presses and orienting movements) or pairs of such (combined orient and lever-press movements; Fig. 4e).

However, DLS activity could reflect sequential organization in other ways<sup>58–60</sup>. For example, it has been proposed that DLS neurons represent the sequential context of movements and actions, including their ordinal position or, in lever-pressing tasks, the identity of the lever being pressed<sup>40</sup>. In such a coding scheme, DLS activity associated with



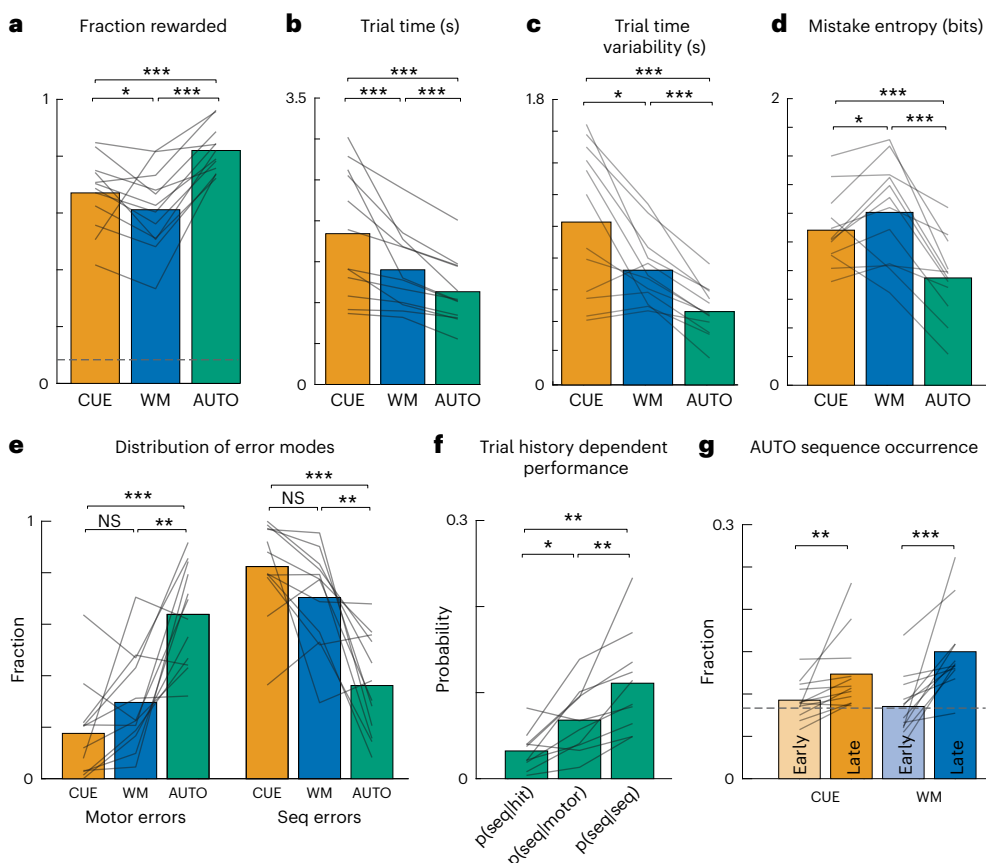


**Fig. 3 | Single overtrained motor sequences show signatures of automaticity.** **a–d**, Performance metrics for the same sequence across tasks at expert performance (Methods). Gray lines are averages within rats; bars are the grand average across rats ( $n = 12$  rats). **a**, Success rate or fraction of rewarded trials. **b**, Median trial duration for rewarded sequences measured as the time from the first to the third lever press. **c**, The s.d. of trial durations. **d**, Variability, or Shannon entropy, of the mistakes made in unrewarded trials (Methods).

**e**, Fraction of unrewarded trials classified as either motor errors or sequence errors (Supplementary Video 2; Methods). **f**, Probability of a sequence error, if the previous trial was rewarded (Hit), a motor error, or a sequence error (Seq), in the AUTO condition. **g**, Probability that the rat performs the automatic sequence in the flexible session before and after the automatic sessions are introduced. Dashed line is the chance of performing any particular sequence (8.33%). For all panels,  $*P < 0.05$ ,  $**P < 0.01$ ,  $***P < 0.001$ , two-sided Wilcoxon signed-rank test.

a specific movement should not be a mere function of its kinematics but also reflect higher-order features of the sequence<sup>25</sup>.

To explicitly probe this, we expanded our analysis to all 12 motor sequences generated in flexible sessions. If DLS represents higher-order features of sequence organization, its neural activity should differ when the same lever-press or orienting movement is performed in different sequential contexts (for example, the press and orienting movement L→C in the sequence L→C→L versus the sequence C→L→C; Fig. 5a). We did not find this to be the case—neural activity across two sequences composed of different elements but similar lever-press and orienting movements was similar (Fig. 5a). More generally, DLS activity associated with a given motor element was highly correlated regardless of the sequence in which it was embedded, its ordinal position in the sequence (first, second and third press), or the specific lever being pressed (that is L, C or R; Fig. 5a–e). There was, however, a very clear distinction in how striatal neurons represented orienting movements to the left and right, both short (for example, L→C) or long (for example, L→R), consistent with an egocentric kinematic code (Fig. 5d,e and Extended Data Fig. 5a,b).

#### DLS encodes detailed movement kinematics

Based on this initial analysis and related studies<sup>15,42,51,61</sup>, a plausible alternative to DLS representing higher-order aspects of discrete motor sequences is that it encodes—and contributes to shaping—the detailed kinematics of learned sequential movement patterns. Although DLS

is not required for species-typical lever-press or orienting movements<sup>15,29,44</sup>, it can, by acting on downstream control circuits, help make them more adapted to a specific task<sup>15,42,62</sup> (Fig. 2e). In this scenario, we would expect DLS neurons to encode kinematic features continuously throughout the behavior<sup>15,50,51</sup>.

To probe this idea<sup>15</sup>, we trained a multilayer neural network to predict, using the spiking activity of simultaneously recorded DLS units, the instantaneous velocity of the rats' active forelimb and nose during the flexible task, as viewed from a side and top camera, respectively (Fig. 5f and Extended Data Fig. 6a). Consistent with observations from trial-averaged ensemble activity, we could decode movement kinematics on individual trials across the different sequences from populations of DLS neurons (Fig. 5g). Decoders trained on a subset of sequences could predict kinematics from held-out sequences just as well (Fig. 5g), implying that the kinematic code in DLS is invariant to the sequential context of the movements as also suggested by our earlier analysis (Fig. 5d,e and Extended Data Fig. 6).

Recent studies<sup>50,63</sup> have suggested that DLS encodes the progression, or ‘phase,’ of a behavioral sequence. In the context of stereotyped movement sequences, however, kinematics and phase are tightly coupled, making it difficult to parse which of these attributes DLS activity reflects<sup>64</sup>. Because our flexible task condition breaks this coupling, kinematics and phase become dissociable. Training a decoder to predict the phase of the behavior, however, failed

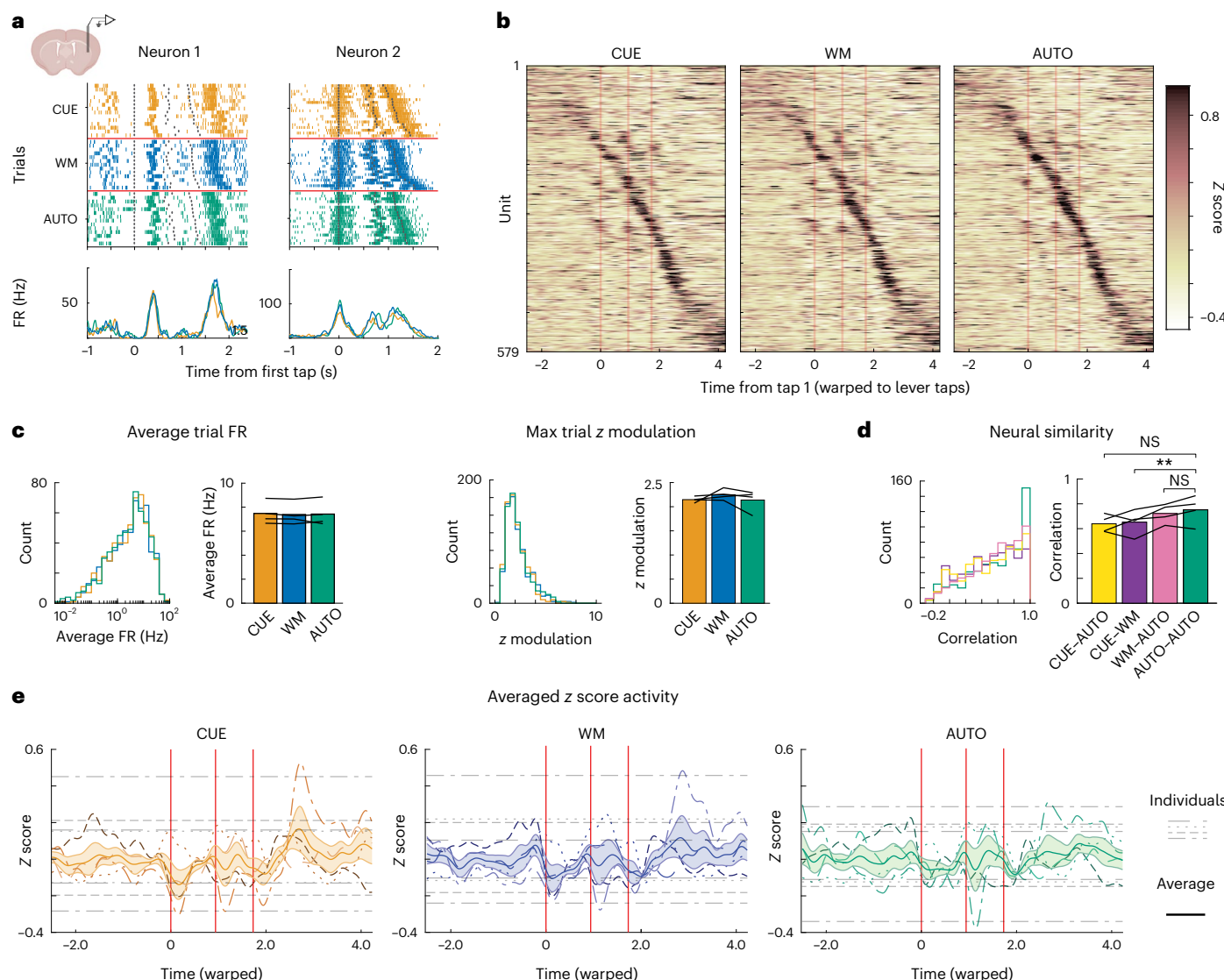


**Fig. 4 | DLS represents motor sequences similarly across task conditions.** **a**, Spike rasters for two example neurons recorded in DLS during the execution of the same motor sequence in CUE (orange), WM (blue) and AUTO (green) trials. Black dots indicate the time of a lever press; red lines separate the task conditions. Below is the instantaneous firing rate across each task condition. Trials were subsampled to have equal trial durations across tasks. **b**, Z-scored average activity of 579 neurons recorded in the DLS during the execution of successful AUTO, CUE and WM trials with the same target sequence (from  $n = 4$  rats). The trials were linearly time-warped to each lever press (red vertical lines). Units were sorted by the time of their peak activity. The sorting index was calculated from half the available trials for each unit, taken from the AUTO trials, and then applied to the remaining trials and task conditions. **c**, Comparing task-aligned activity statistics across the population of recorded neurons. Left, histogram of the average firing rate during the trial period ( $P > 0.05$ , paired two-sided  $t$  test for each task condition). The bar graph breaks this down by rats ( $n = 4$ ). Right, same as in the left panel but for maximum modulation of

z-scored firing rate during the trial period ( $P = 0.94$  AUTO–CUE,  $P = 0.25$  AUTO–WM,  $P = 0.26$  CUE–WM, paired two-sided  $t$  test). **d**, Histogram of correlation coefficients between trial-averaged activity across task conditions for the DLS neurons shown in **b** (Methods). Left, histogram of the correlation coefficients of the trial-averaged neural activity on CUE and AUTO trials (yellow), CUE and WM trials (purple), WM and AUTO trials (pink) and AUTO and a held-out set of AUTO trials (green). Right, mean correlation coefficients for trial-averaged activity across task conditions broken down by animal ( $n = 4$ ). \*\* $P < 0.01$ , paired two-sided  $t$  test. **e**, Z-scored firing rates averaged over all neurons. Thick, solid lines indicate the grand average across all rats ( $n = 4$ ), and colored shaded regions indicate the s.e.m. across rats. Thin, dashed lines indicate individual rats, and the thin, dashed gray lines denote the 95% confidence interval of z-scored activity. Average firing rates are highly correlated across all tasks for each rat (Pearson correlation of  $0.8286 \pm 0.0874$ , mean  $\pm$  s.e.m) and do not significantly differ at the time of the first lever press ( $P > 0.05$ , two-sided  $t$  test,  $n = 4$  rats). FR, firing rate.

(Fig. 5h), meaning that phase in the sequence cannot be recovered from DLS activity alone. Only when phase and kinematics were coupled, that is, when we considered only single sequences with no repeated motor elements (for example, lever taps; see Methods for how these were selected), could we decode phase (Fig. 5h). Taken together, our results suggest that DLS encodes low-level continuous kinematics of movements in a way that is—in contrast to prior reports<sup>40,41</sup>—invariant to their sequential context.

### Probing DLS function by lesions

Although our neural recordings showed that DLS activity reflects ongoing kinematics in a similar way for sensory-guided, working memory-guided and automatic motor sequences, this does not establish a causal role for DLS in their execution. Alternatively, DLS activity could—in one or all task conditions—simply reflect input from essential sensorimotor control circuits<sup>18</sup>. To arbitrate between these possibilities, we lesioned DLS bilaterally in expert animals ( $n = 7$  rats; Methods; Fig. 6a and Extended Data Fig. 3b).

In interpreting the effects of striatal lesions, we distinguish, as we did for the neural analysis, two aspects of performance, each associated with a putative function of the BG (Fig. 6b). The first is the ability to perform the prescribed sequence of lever presses (that is, ‘sequencing’). The second is the ability to use fast and efficient movements refined and adapted to the task (that is, ‘kinematics’). Note that only the sequencing aspect is required for reward. Parsing performance in this way allowed us to probe whether the striatum contributes to high-level sequence structure and low-level movement kinematics differently across task conditions.

### DLS lesions affect high-level sequence structure on automatic and working memory-guided, but not visually cued, trials

Following a 7-d postlesion recovery (Methods), the rats’ ability to perform the AUTO sequence was severely impaired (Fig. 6c,d), dropping to near chance levels (8.33%). In stark contrast, success rates on CUE sequences were comparable to prelesion (Fig. 6c,d), save for a brief drop in the first few sessions after the lesions, consistent with nonspecific transient effects of the surgery<sup>15,16</sup>. Success rates in WM trials, on the other hand, were chronically affected with performance dropping to near chance levels (Fig. 6c,d) and changing significantly more than CUE performance ( $P=0.015625$ , Wilcoxon two-sided signed-rank test,  $n=7$  rats). A 7-d control break before the lesion (Methods) did not substantially affect the behavior in either task condition (Extended Data Fig. 7).

One possible explanation for the lesion resilience in CUE trials, as well as the less severe performance drop in WM trials (compared to AUTO), is that visual cues aid movement initiation in a DLS-independent manner. However, the postlesion drop in success rate on AUTO and WM trials could not be explained by a deficit in movement initiation<sup>42</sup>. Although DLS-lesioned rats generated fewer lever presses overall, they were actively engaged in the task and performed similar numbers of trials across flexible and automatic sessions (Extended Data Fig. 8a).

Taken together, these results are consistent with DLS having an essential role in controlling the sequence structure for automatic and working memory-guided motor sequences<sup>15,54</sup>. However, DLS is dispensable for sequencing visually cued behaviors.

### DLS lesions affect learned movement kinematics equally across task conditions

Consistent with a general role for the BG in specifying learned task-specific movement kinematics<sup>15</sup>, we found that orienting and lever-pressing movements across all three tasks were affected to a similar degree. The ‘vigor’ of the movements, defined as the scalar gain factor applied to the kinematic features of a movement such

as movement latency or speed<sup>62,65,66</sup>, was also reduced (Fig. 6e,f and Extended Data Fig. 9).

One plausible coupling between deficits in kinematics/vigor and the ability to generate the proper sequence is if the neural dynamics that inform the sequence in AUTO and WM trials can be expressed only at higher (that is, closer to prelesion) speeds (CUE trials would be paced and informed by visual cues and hence would not be affected). Under this hypothesis, successful postlesion trials should be performed with similar speeds to prelesion trials. We saw no evidence for this (Fig. 6e,f and Extended Data Fig. 9e–g).

Another interpretation is that DLS lesion-induced reduction in vigor reflects a change in sensitivity to effort or motivation<sup>61,66</sup>. Because overtrained behaviors are thought to be less sensitive to effort<sup>62</sup>, the expectation is that lesions would impact the speed, success or overall engagement of AUTO trials less than CUE or WM trials. Given that we observed similar relative decreases in vigor across all task conditions (Fig. 6e,f) and similar levels of engagement in both session types postlesion (Extended Data Fig. 9a), it suggests that the reduction in vigor is not due to a change in motor motivation.

Although the lesion-induced effects on overall movement speed and latency are consistent with prior reports on BG’s role in controlling movement vigor<sup>23,61</sup>, other aspects of kinematics were also affected. Trial-to-trial movement variability, even for similar duration movements, was dramatically increased (Fig. 6g,h). Furthermore, the smoothness of task-related movements, which increases over learning<sup>46</sup>, also decreased following DLS lesions (Fig. 6i). Comparing the effects on vigor to these, more fine-grained aspects of kinematics showed that they were largely uncorrelated, consistent with DLS affecting vigor and more fine-grained aspects of kinematics independently (Extended Data Fig. 9h).

Interestingly, we found that the quality of the movements postlesion reverted to what is seen early in learning (Extended Data Fig. 8b–g). This suggests that the basic movements that form the building blocks of the animal’s task-relevant behavior are controlled by circuits downstream of the BG (likely brainstem)<sup>67</sup> and that the sensorimotor arm of the BG adds learned task-specific kinematic refinements to these species-typical motor programs<sup>17</sup>.

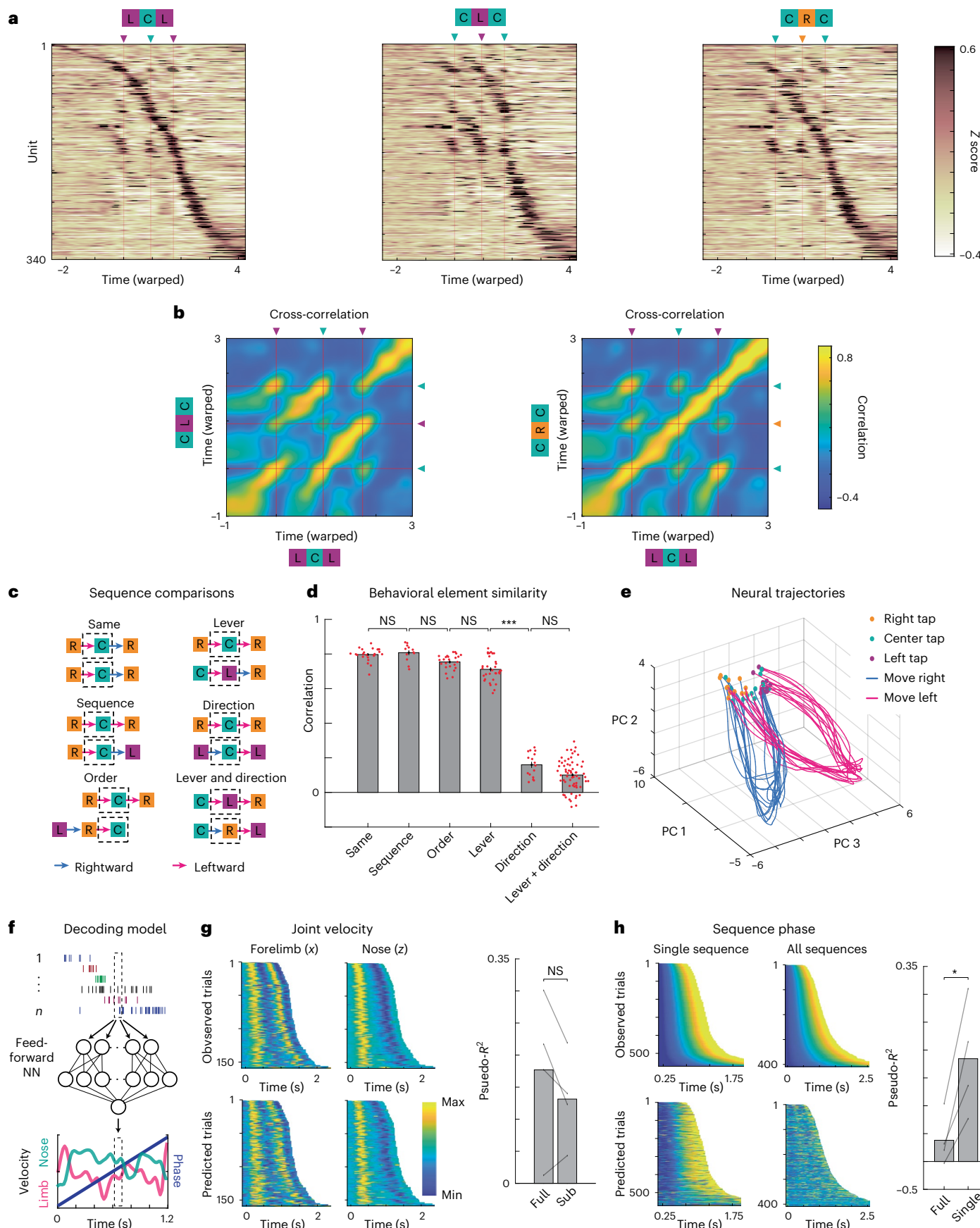
### The dorsomedial striatum (DMS) is not required for motor sequence execution in either task condition

Our focus on sensorimotor striatum (DLS) was motivated by its known role in movement execution<sup>62,68</sup>. In contrast to DLS, which receives much of its input from the sensorimotor cortex, DMS receives its cortical input predominantly from the prefrontal cortex and posterior parietal cortex<sup>69</sup>. Although this associative region of the striatum has

**Fig. 5 | DLS encodes low-level kinematics, not high-level attributes, of discrete motor sequences.** **a**, Comparing trial-averaged neural activity for different sequences, from all DLS neurons that met our criteria for inclusion (Methods), across four rats. Units were sorted based on the time of peak firing rate in the LCL sequence (leftmost). Sequences LCL and CLC (left and center) comprise the same motor elements (LC and CL occur in both), but ordered differently. Sequences LCL (left) and CRC (right) comprise the same actions (press, move right, press, move left, press), but on different levers. **b**, Cross-correlations of time-varying neural activity from **a** (Methods). **c**, The flexible condition allows us to compare the same sub-sequence of orienting and pressing movement (here, rightward orienting and pressing) in different sequential contexts. Dashed box indicates examples of comparisons made in **d**. **d**, Correlation of the neural activity patterns associated with the same sub-sequence of orienting and pressing movements in different sequential contexts ( $n=24, 12, 24, 32, 16, 64$  different lever presses for each bar from left to right). Error bars denote s.e.m. \*\*\* $P<0.001$ , Bonferroni-corrected two-sided Wilcoxon rank-sum test. **e**, Neural population trajectories in PC space for the 12 different sequences, plotted along the first, second and third PC. In DLS, all lever-press movements (color dots) are associated with similar neural activities, as are all rightward (blue) and leftward (magenta) movements, independent of lever identity or order in the sequence (that is, right→center, center→left and right→left

are all similar). **f–h**, Decoding analysis. **f**, Schematic of the decoding analysis. A feed-forward neural network was trained to predict either the instantaneous velocity of the active forelimb (viewed from the side) and the nose (viewed from above), or the sequence phase, from the spiking activity of groups of simultaneously recorded DLS units. **g**, Velocity of the active forelimb (top-left) and nose (top-right) from a representative session, in the +x and +z dimensions, respectively (Methods). Trials are aligned to the first lever press and sorted by trial duration. Velocity predictions on held-out trials for forelimb (bottom left) and nose (bottom right). Right, model performance (measured in pseudo- $R^2$ ; Methods), tested on held-out trials, when predicting all velocity components (forelimb +x, +y and nose +x, +z; Methods). Performance is shown for models trained on every sequence (full) and tested on held-out trials and for models trained on a randomly selected half of the sequences and tested on the other half (subset). Gray lines indicate model performance within individual rats ( $n=4$ ). **h**, Heatmaps show the observed (top) and predicted (bottom) sequence phases for single sequences without repeated elements (left) and for all flexible sequences (right). Trials are aligned to the first tap. Right, model performance, tested on held-out trials and quantified by the pseudo- $R^2$ , for models trained on all flexible sequences (full) and those trained on a single sequence with nonrepeating elements (single). Lines indicate performance for individual rats ( $n=4$ ). \* $P<0.05$ , two-sided  $t$  test. NN, neural network.

been implicated in flexible control of behavior, such as modifying, switching and updating behavioral choices in response to previously learned associations<sup>70,71</sup>, whether it has an essential role in generating sensory- or WM-guided motor sequences is less clear<sup>29,44</sup>. To probe this, we lesioned DMS bilaterally in a separate cohort of expert animals ( $n=6$  rats; Methods; Fig. 7a and Extended Data Fig. 3c).



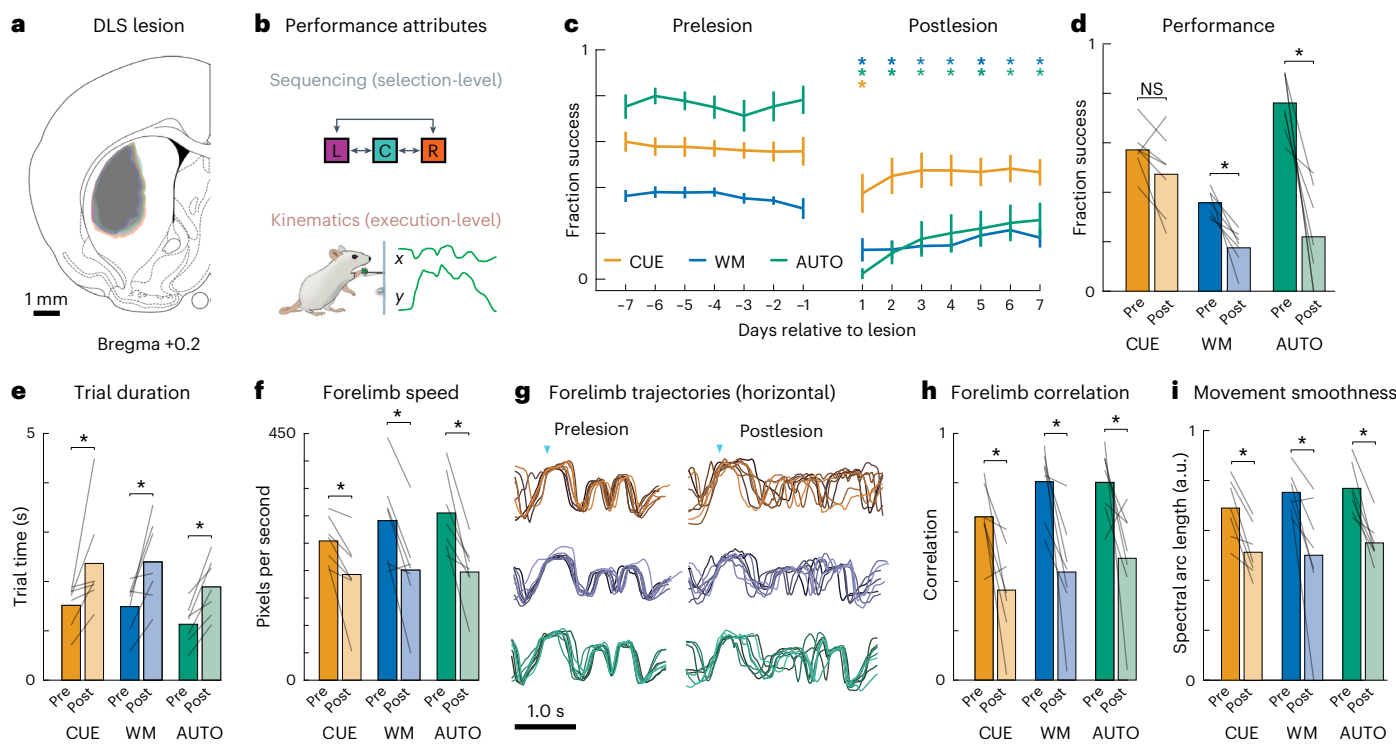


**Fig. 6 | DLS is required for generating task-specific movement kinematics across all task conditions but it is not required for ordering basic movements in the prescribed sequence when visually cued.** **a**, Outline of DLS lesion boundaries from three rats in one hemisphere. For full lesion annotation, see Extended Data Fig. 3b. **b**, Schematic of the two performance attributes we parse. The first is high-level sequencing of orienting and pressing movements. Success (reward) in the task is contingent on getting this right. The second is the low-level implementation of the requisite movements, that is, task-specific learned kinematics. Although movements adapted to the task are faster and more fluid than at the onset of training, they are not required for reward. **c,d**, Effects of DLS lesions on sequencing. **c**, Success rate in producing the prescribed sequence, averaged over rats ( $n = 7$ ; error bars are s.e.m.), in the week before and after lesion. Stars denote whether performance is significantly different on a given day, relative to average performance in the week before the lesion, for each task

condition. **d**, Bars show success rate in the week before and days 3–7 after the lesion, averaged across rats ( $n = 7$ ). Gray lines denote individual rats. **e–i**, Effects of DLS lesions on movement kinematics. **e**, Trial times. **f**, Average forelimb speed for successful trials before and after the lesions, across rats ( $n = 7$ ; Methods). The relative change due to lesion is similar across trial types for both trial times ( $P = 0.3750$  CUE versus WM,  $P = 0.2969$  CUE versus AUTO,  $P = 0.8125$  WM versus AUTO) and forelimb speeds ( $P = 0.2969$  CUE versus WM,  $P = 0.1565$  CUE versus AUTO,  $P = 0.6875$  WM versus AUTO). **g**, The horizontal (x) position of the active forelimb on eight example trials with similar duration is overlaid and compared before (left) and after (right) DLS lesions. **h**, Average trial-to-trial correlation. **i**, Movement smoothness for trajectories of the active forelimb (both horizontal (x) and vertical (y)) before and after lesion ( $n = 7$  rats). For all panels,  $^*P < 0.05$ , two-sided Wilcoxon signed-rank test.

Consistent with prior work<sup>15</sup>, DMS was not required for automatic motor sequence execution (Fig. 7b,c). More surprisingly, DMS lesions also did not have any lasting effects on flexible motor sequence execution in either WM or CUE trials (Fig. 7d–h). Furthermore, unlike for DLS, lesions of DMS did not significantly affect kinematic metrics in either task condition, with lesioned rats showing no consistent increase in trial time or mean trial speed or a drop in the stereotypy of their task-related movements (Fig. 7d–h). This reinforces the dissociation between the DLS and DMS in terms of low-level kinematic control<sup>15</sup> and further suggests that DMS is not necessary for either sequencing or kinematic aspects of well-trained motor sequences. Whether DMS has a role in early motor sequence learning remains an intriguing open question<sup>27–29,72</sup>.

### A simple neural network model can account for the results in both CUE and AUTO tasks

At first glance, our results suggesting both similar (for example, in terms of coding properties and contribution to low-level kinematics) and different (for example, in terms of effects of lesions on high-level sequence structure) functions for DLS across tasks may seem discrepant. To reconcile these findings and better inform the circuit-level logic underlying motor sequence execution, we built a simple neural network model of the motor system (Fig. 8a) in which a DLS-like circuit learns to

interact with ‘downstream’ control circuits under different task conditions. Our modeling focused on the sensory-guided and automatic tasks, as these show the clearest distinctions in our experimental data, setting aside for this analysis the WM-driven condition.

The DLS network in our model contained no recurrence, reflecting the fact that MSNs are coupled via relatively weak and sparse lateral inhibition<sup>73</sup>. The ‘downstream’ component of the model—intended to capture the control circuits modulated by the BG—was made recurrent. For simplicity, and to focus on the DLS, we abstracted away the details of how it connects to downstream control circuits (that is, through other BG nuclei, thalamus, etc.), modeling them with a set of linear synaptic weights. To capture the ability of animals to execute cued lever presses before sequence training, we pretrained our model to perform a simple *in silico* version of ‘lever-pressing’—moving a virtual manipulandum to a target in a 2D environment (Methods).

We then trained the DLS input synapses such that the network’s output ‘moved’ through sequences of three targets (Fig. 8b; Methods). The same network was tasked with producing sensory-guided sequences instructed by external inputs (CUE task), as well as a single internally generated sequence (AUTO task; Methods).

Because animals value time<sup>74</sup> and reduce trial duration as a function of learning (Fig. 2d), our training procedure incentivized the model to reach the three target positions in the correct order as quickly as

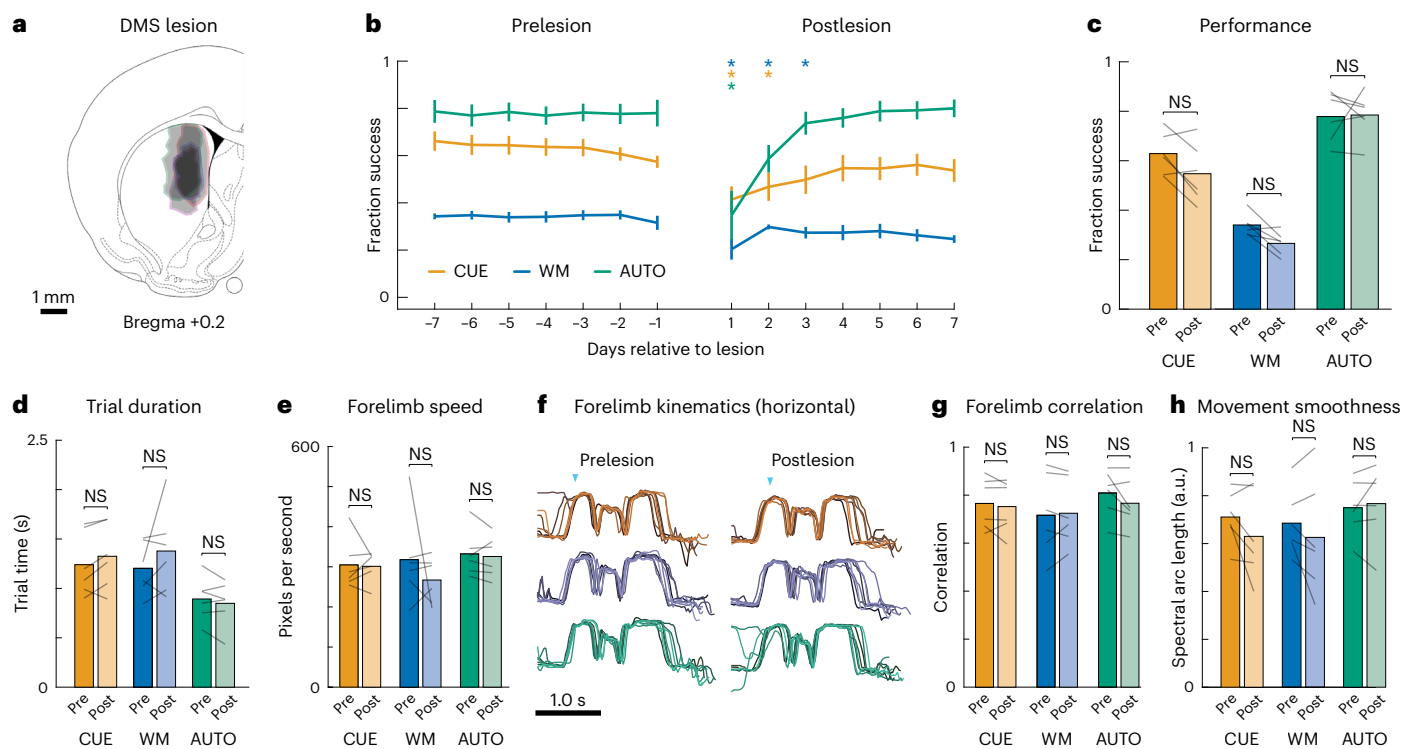


**Fig. 7 | DMS lesions have no long-term effect on either flexible or automatic sequence execution.** **a**, Outline of DMS lesion boundaries, from three rats in one hemisphere. For full lesion annotation, see Extended Data Fig. 3c. **b,c**, Effects of DMS lesions on sequencing. **b**, Success rates in producing the prescribed sequence, averaged over rats ( $n = 6$ ; error bars are s.e.m.), in the week before and after lesion. Stars denote whether performance is significantly different on a given day, relative to average performance in the week prelesion, for each task condition. **c**, Bars show success rate in the week prelesion and days 3–7 postlesion,

averaged across rats ( $n = 6$ ). Gray lines denote individual rats. **d–h**, Effects of DMS lesions on movement kinematics. **d**, Trial times. **e**, Average forelimb speed before and after the lesions (Methods;  $n = 6$  rats). **f**, The horizontal ( $x$ ) position of the active forelimb on eight example trials, from one rat, with similar durations is overlaid and compared shown before (left) and after (right) DMS lesions. **g**, Average trial-to-trial correlation. **h**, Movement smoothness for trajectories of the active forelimb (both horizontal ( $x$ ) and vertical ( $y$ )) before and after lesion ( $n = 6$  rats). For all panels,  $P > 0.05$ , two-sided Wilcoxon signed-rank test.

possible. The decision to train the DLS input synapses was inspired by the presumed role of cortico-striatal and thalamo-striatal plasticity in reinforcement learning<sup>17,75</sup>.

To compare the performance of our network model to that of real rats, we conducted analyses of the model analogous to those performed on our experimental data. We found that the activity of the neural units in the trained DLS network was largely independent of task condition as seen in our data (Fig. 8c,d; compare with Fig. 4b,d). This independence reflects an emergent alignment of DLS inputs (which are trained on both tasks) for AUTO and CUE trials with the same target sequence (Fig. 8e). We also recapitulated our experimental observation that DLS network representations reflected egocentric direction-of-motion information (Fig. 8f; compare with Fig. 5d,e).

Next, we simulated lesions to the DLS by removing this part of the model following training, comparing the effects on sequencing and kinematics separately. We found that DLS removal left high-level sequencing impaired for AUTO but not CUE trials (Fig. 8g; compare with Fig. 6a), recapitulating our experimental results. The model also captured the effect of DLS lesions on movement trajectories, decreasing movement velocity and increasing trial time across execution modes. This is consistent with a role for DLS in adapting movement kinematics independent of task condition (Fig. 8h,i; compare with Fig. 6a,b).

Thus, key features of the experimental data—*invariance of DLS activity to task condition, sensitivity of automatic task performance to DLS lesion and a role for DLS activity in shaping learned movement kinematics—all emerge naturally during task learning when using a network model with BG-like circuitry.*

In the model, we used a biologically inspired circuit architecture (Fig. 8a) and matched the training procedure of the network to that of our rats (that is, with sequence training overlaid on pretrained circuits). To probe how different features of our model contributed to the results, we also considered three alternative circuit models/paradigms. First, to test whether our results depended on DLS output being time-varying and high-dimensional, so as to specify detailed kinematics, we made the DLS output scalar, thus constraining it to represent coarse sequence-level information, for example, movement speed modulation or ‘vigor,’ as has been suggested<sup>23,61</sup>. This modelled to markedly different DLS activity patterns across execution modes, in violation of our experimental findings (Extended Data Fig. 10a–g).

We next explored an ‘action-selection’ model in which DLS is constrained to generate signals only at the boundaries of elementary movements, which inform the rest of the circuit of the next ‘lever-press’ to be executed. This model resulted in DLS activity patterns that lacked prominent representations of egocentric movement information, again in violation of our experimental data (Extended Data Fig. 10h–m). Finally, to test whether the task-specific deficits of our lesions were due to the existence of pretrained motor circuits capable of executing cued movements, we eliminated the pretraining of downstream circuits and trained the full network de novo on all aspects of both task conditions (CUE and AUTO). This simulation failed to capture the DLS lesion resilience seen in our experiments (Extended Data Fig. 10n–s).

Comparing the results from our various models with our experimental data further supports the idea that, for behaviors with learned

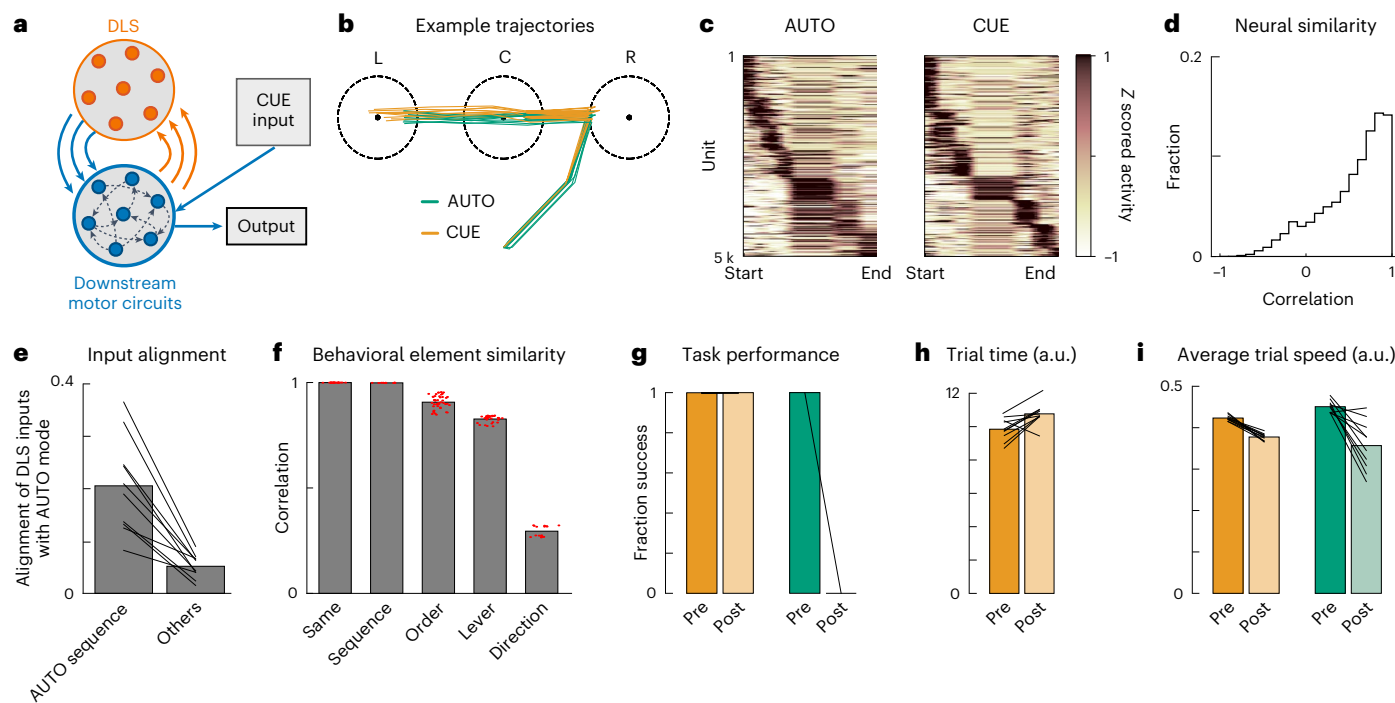


**Fig. 8 | Experimental results emerge naturally during task learning in a dual module neural network model.** **a**, Schematic illustrating the architecture of our neural network model. DLS weights (orange) are trained on the cued and automatic tasks and interact with downstream recurrent motor circuits already trained to perform cued movements. **b**, Example trajectories on the simulated task. The network controls the velocity of a 'forelimb' and must move it into three circular regions (representing 'level-presses') in the correct sequential order (in this example, the sequence right-center-left (RCL) for both the CUE and AUTO modes). **c**, Average z-scored activity of model neurons in the DLS population during the execution of successful AUTO and cued trials with the same target sequence. Neurons are sorted by the time of their peak activity and displayed in the same order in both plots. **d**, Histogram of correlation coefficients between CUE and AUTO tasks over all model DLS neurons of correlation, as in Fig. 4d.

**e**, Correlation between input to DLS units across tasks. Line segments indicate individual simulations; bars indicate averages across simulations ( $n = 10$  runs). Left bar, correlation between DLS inputs on AUTO and cued trials for the same sequence. Right bar, same measurement but shown for cued trials with other target sequences (averaged over all other sequences). **f**, Correlation of the neural activity patterns associated with the same sub-sequence of orienting and pressing movements in different sequential contexts, as in Fig. 5d. **g**, Effects of DLS removal on sequencing. Average success rate in producing the prescribed sequence. Averaged across ten network simulations for each condition. Lines depict individual simulations. **h,i**, Effects of DLS removal on kinematics. **h**, Trial time (that is, number of simulation steps). **i**, Average trial speed (average magnitude of velocity, in arbitrary simulation units) averaged across ten network simulations for each condition.

task-specific kinematics, the BG provide fine-scale kinematic control signals to downstream circuits, which in the case of automatic motor sequences defines the high-level sequential structure of the learned behavior.

## Discussion

We set out to probe the BG's contribution to motor sequence execution and how it differs depending on whether the sequence is informed by sensory cues, working memory, or is generated automatically after lengthy overtraining (Fig. 1). Surprisingly, neural activity patterns in the sensorimotor striatum (DLS) of rats producing the same three-element sequences were similar across the different task conditions (Figs. 2–4), representing low-level kinematic features of the behaviors (Fig. 5). Consistent with this coding scheme, lesions to the DLS affected task-specific movement kinematics similarly in all tasks. Interestingly, higher-level sequential organization, while not represented in DLS, was affected by DLS lesions on overtrained and working memory-guided trials but remained intact for visually cued sequences (Fig. 6). Lesions to the associative regions of the striatum (DMS) had only transient effects on performance and no effect on movement kinematics (Fig. 7). A simple network model could recapitulate our results and provide an explanation for the different findings—DLS learns to transform its inputs into task-invariant activity patterns that provide similar kinematic control signals to downstream motor circuits in all task conditions (Fig. 8).

## DLS's role in specifying low-level kinematics of task-specific learned movements

The BG have been implicated in a diverse array of functions related to motor sequence execution, including action selection<sup>26,60,76</sup>, the storage of sensorimotor associations<sup>15,18</sup>, chunking<sup>76</sup> and low-level kinematic specification of the requisite movements<sup>15,23,42,51</sup>. Evidence for the different functions comes from studies that challenge animals to produce motor sequences in different ways<sup>11</sup>, some relying on sensory cues and others on working memory to inform sequencing<sup>54,55,59</sup>, while many probe overtrained, or automatic, sequence execution<sup>15,28,40,41,50</sup>. Thus, the often-discrepant views of BG's role in motor sequence execution could simply reflect the different computational demands of the various tasks and BG's ability to contribute to each of them in different ways and to different degrees.

Our experimental paradigm allowed us to test this by probing striatal function across three distinct task conditions of motor sequence execution in the same animal and across the same neural populations. Surprisingly, we did not find any meaningful difference in DLS activity when animals performed the same motor sequence in the different task conditions, representing egocentric movement kinematics in all cases<sup>15,42,50,51,62</sup>.

Consistent with the role of the DLS in specifying fine-grained time-varying kinematics of acquired behaviors, lesions affected task-specific learned movements across the task conditions (Fig. 6e,f). While lesioned animals could still orient toward the levers and press

them, the speed and variability of their movements reverted to what they expressed early in learning (Extended Data Fig. 8b–f), consistent with the results from an earlier study<sup>15</sup>.

Together, these results implicate the DLS in the task-specific refinement of species-typical movements generated in downstream control circuits, in our case, likely in the brainstem<sup>67</sup>. We saw a similar result in our circuit model—when the ‘DLS’ circuit was allowed to interact with pre-trained ‘downstream circuits’ that could independently respond to cues, variability in trial duration decreased following sequence learning and increased following DLS lesion for both automatic and cued execution modes (Fig. 8h,i). Dissecting the model revealed that, despite receiving different inputs across modes, the DLS learned task-invariant activity that modulated movement kinematics by acting on its downstream targets.

### DLS’s role in generating high-level sequential structure

Despite our experiments implicating the BG in the specification of task-specific movement kinematics<sup>15,42,50</sup>, successful performance in our task does not explicitly require such adapted kinematics. Reward is contingent only on the three-element sequence being generated as prescribed, which can be done also with slow and inefficient movements akin to what DLS-lesioned animals express. Therefore, deficits in task performance after DLS lesions would seem to implicate it also in the control of high-level sequence structure.

However, we found no evidence for DLS activity representing such sequence structure. Furthermore, while DLS lesions severely affected performance in automatic and working memory-guided sessions, there was no substantial lasting effect on the success rate in visually cued trials despite the kinematics being similarly affected. Interestingly, this dissociation mirrors what is seen in patients with Parkinson’s disease, whose inability to execute internally generated motor sequences can be rescued by providing instructive visual or auditory cues<sup>19</sup>. Intriguingly, much like we see in our lesioned rats, patients with Parkinson’s disease exhibit kinematic deficits, including in movement vigor, independently of the patient’s ability to move accurately<sup>66</sup>. Taken together with our results, this implies that the BG need not be essential for expressing cue-action associations or the serial action-selection process they inform but provide kinematic refinement to the requisite movements.

That DLS lesions affected sequence structure on trials in which the prescribed sequence was not informed by external cues (AUTO and WM trials) raises the question of how the DLS, and the BG more generally, contributes to sequencing such internally generated behaviors. For highly stereotyped overtrained motor sequences (expressed on AUTO trials), we posit that the behavior becomes consolidated in terms of DLS-dependent continuous low-level kinematics<sup>9,25</sup>. In this case, behavioral progression would no longer rely on the selection of discrete actions but instead results from an invariant and continuous mapping of past-to-future behavior, a process we argue is DLS dependent<sup>11,15</sup>.

### DLS’s role in ‘chunking’ and action selection

The BG have also been widely implicated in the process of ‘chunking’<sup>76</sup>, through which a motor sequence initially generated by a serial decision-making process becomes linked, over the course of training, in a way that allows the sequence to be selected and executed as a single action<sup>76</sup>. Support for BG’s role in chunking comes from studies showing that the neural representation of task-specific motor sequences in the striatum becomes sparser with extended practice<sup>56,77</sup>, preferentially marking the boundaries (that is, start and stop) of overtrained, or ‘chunked,’ behaviors<sup>40,41,56</sup>. Such sparsification is consistent with a role for the BG in selecting actions elaborated in downstream circuits<sup>56,77</sup>. For sensory- and working memory-guided behaviors, action selection would occur at the level of individual elements and hence be more granular, while selection for overtrained behaviors would happen at the level of the whole sequence or ‘chunk’.

Our paradigm allowed us to directly probe whether DLS activity reflects such a function by comparing it for the same motor sequence

with similar kinematics in an automatic (selection of the sequence as a chunk) and a flexible (serial selection of discrete motor elements) context (Fig. 1). Not only did we fail to see prominent start/stop activity on automatic trials, but we also found that flexible and automatic motor sequences share highly correlated representations in the DLS (Fig. 4).

How should the differences between our results and those showing signatures of chunking and—implicitly—the selection of overtrained sequences by the BG be interpreted? First, most studies implicating BG in chunking tend to compare overall activity early in learning to what is seen in the expert (for example, refs. 27,53,57,77). Any observed activity difference could thus reflect either the process of chunking or changes in movement kinematics that occur as a function of training. For example, one recent study found behaviorally locked sequential activity patterns in DLS already early in learning, while position- and speed-related activity became more prominent after extensive practice<sup>50</sup>. That we see no difference across automatic and flexible motor sequences suggests that start/stop and sequence-specific activity seen in previous studies is not the consequence of motor chunking per se but may instead reflect learning-related changes in motor output or a shift in how the DLS contributes to it.

Alternatively, the lack of sequence-specific activity in our study could mean that the motor sequence we overtrained failed to coalesce into a single ‘chunk’ due to some peculiarity of our experimental approach. We do not find this plausible, given the clear signatures of automaticity we see (Fig. 3) and the lengthy training times. Furthermore, in an earlier study, in which we trained rats to generate highly stereotyped and stable movement patterns without any need for serial decision-making or action selection, we similarly did not see start/stop activity<sup>15</sup>.

While our results do not support a role for the BG in initiating consolidated motor chunks elaborated downstream, they are consistent with overtrained motor sequences becoming defined as BG-dependent motor chunks. Thus, rather than selecting them, BG’s role in motor chunking could be in transforming discrete motor sequences into single continuous actions in which the high-level sequential structure of the overtrained behavior is specified by BG-dependent low-level kinematics.

### Circuits controlling sensory-guided motor sequences need to be elucidated

Our finding that visually guided motor sequences can be performed, as prescribed after DLS and DMS lesions, begs the question of which circuits control the progression of externally cued behaviors. Work in humans and NHPs have suggested a role for cortex<sup>22,30,78</sup>. Although we have shown that the motor cortex is not required for executing highly overtrained automatic behaviors in rodents<sup>16</sup>, it remains an open question whether and how the motor cortex contributes to sensory-guided motor sequences and the degree to which its function differs across task conditions. Future experiments will be needed to address the degree to which the motor cortex’s contributions to movement control depend on the specific challenges posed by a task, and the condition under which its function requires the BG.

### Online content

Any methods, additional references, Nature Portfolio reporting summaries, source data, extended data, supplementary information, acknowledgements, peer review information; details of author contributions and competing interests; and statements of data and code availability are available at <https://doi.org/10.1038/s41593-023-01431-3>.

### References

1. Schneider, W. & Shiffrin, R. M. Controlled and automatic human information processing: I. Detection, search, and attention. *Psychol. Rev.* **84**, 1–66 (1977).
2. Pashler, H. Dual-task interference in simple tasks: data and theory. *Psychol. Bull.* **116**, 220–244 (1994).

3. Wiestler, T. & Diedrichsen, J. Skill learning strengthens cortical representations of motor sequences. *eLife* **2**, e00801 (2013).
4. Wymbs, N. F. & Grafton, S. T. The human motor system supports sequence-specific representations over multiple training-dependent timescales. *Cereb. Cortex* **25**, 4213–4225 (2015).
5. Ashby, F. G., Turner, B. O. & Horvitz, J. C. Cortical and basal ganglia contributions to habit learning and automaticity. *Trends Cogn. Sci.* **14**, 208–215 (2010).
6. Karni, A. et al. The acquisition of skilled motor performance: fast and slow experience-driven changes in primary motor cortex. *Proc. Natl Acad. Sci. USA* **95**, 861–868 (1998).
7. Ramkumar, P. et al. Chunking as the result of an efficiency computation trade-off. *Nat. Commun.* **7**, 12176 (2016).
8. Wu, T., Kansaku, K. & Hallett, M. How self-initiated memorized movements become automatic: a functional MRI study. *J. Neurophysiol.* **91**, 1690–1698 (2004).
9. Haith, A. M. & Krakauer, J. W. The multiple effects of practice: skill, habit and reduced cognitive load. *Curr. Opin. Behav. Sci.* **20**, 196–201 (2018).
10. Sun, M.-K. (ed.) *Advances in Cognitive and Behavioral Sciences* 141–159 (Nova Science Publishers, 2014).
11. Kadmon Harpaz, N., Hardcastle, K. & Ölveczky, B. P. Learning-induced changes in the neural circuits underlying motor sequence execution. *Curr. Opin. Neurobiol.* **76**, 102624 (2022).
12. Doyon, J. et al. Contributions of the basal ganglia and functionally related brain structures to motor learning. *Behav. Brain Res.* **199**, 61–75 (2009).
13. Hikosaka, O. et al. Parallel neural networks for learning sequential procedures. *Trends Neurosci.* **22**, 464–471 (1999).
14. Matsuzaka, Y., Picard, N. & Strick, P. L. Skill representation in the primary motor cortex after long-term practice. *J. Neurophysiol.* **97**, 1819–1832 (2007).
15. Dhawale, A. K., Wolff, S. B. E., Ko, R. & Ölveczky, B. P. The basal ganglia control the detailed kinematics of learned motor skills. *Nat. Neurosci.* **24**, 1256–1269 (2021).
16. Kawai, R. et al. Motor cortex is required for learning but not for executing a motor skill. *Neuron* **86**, 800–812 (2015).
17. Wolff, S. B. E., Ko, R. & Ölveczky, B. P. Distinct roles for motor cortical and thalamic inputs to striatum during motor skill learning and execution. *Sci. Adv.* **8**, eabk0231 (2022).
18. Robbe, D. To move or to sense? Incorporating somatosensory representation into striatal functions. *Curr. Opin. Neurobiol.* **52**, 123–130 (2018).
19. Redgrave, P. et al. Goal-directed and habitual control in the basal ganglia: implications for Parkinson's disease. *Nat. Rev. Neurosci.* **11**, 760–772 (2010).
20. Poldrack, R. A. et al. The neural correlates of motor skill automaticity. *J. Neurosci.* **25**, 5356–5364 (2005).
21. Xu, D. et al. Cortical processing of flexible and context-dependent sensorimotor sequences. *Nature* **603**, 464–469 (2022).
22. Mushiake, H., Inase, M. & Tanji, J. Neuronal activity in the primate premotor, supplementary, and precentral motor cortex during visually guided and internally determined sequential movements. *J. Neurophysiol.* **66**, 705–718 (1991).
23. Desmurget, M. & Turner, R. S. Motor sequences and the basal ganglia: kinematics, not habits. *J. Neurosci.* **30**, 7685–7690 (2010).
24. Berlot, E., Popp, N. J. & Diedrichsen, J. In search of the engram, 2017. *Curr. Opin. Behav. Sci.* **20**, 56–60 (2018).
25. Diedrichsen, J. & Kornysheva, K. Motor skill learning between selection and execution. *Trends Cogn. Sci.* **19**, 227–233 (2015).
26. Geddes, C. E., Li, H. & Jin, X. Optogenetic editing reveals the hierarchical organization of learned action sequences. *Cell* **174**, 32–43 (2018).
27. Miyachi, S., Hikosaka, O. & Lu, X. Differential activation of monkey striatal neurons in the early and late stages of procedural learning. *Exp. Brain Res.* **146**, 122–126 (2002).
28. Miyachi, S., Hikosaka, O., Miyashita, K., Karádi, Z. & Rand, M. Differential roles of monkey striatum in learning of sequential hand movement. *Exp. Brain Res.* **115**, 1–5 (1997).
29. Yin, H. H. The sensorimotor striatum is necessary for serial order learning. *J. Neurosci.* **30**, 14719–14723 (2010).
30. Tanji, J. Sequential organization of multiple movements: involvement of cortical motor areas. *Annu. Rev. Neurosci.* **24**, 631–651 (2001).
31. Jin, X. & Costa, R. M. Shaping action sequences in basal ganglia circuits. *Curr. Opin. Neurobiol.* **33**, 188–196 (2015).
32. Abrahamse, E. L., Ruitenberg, M. F. L., de Kleine, E. & Verwey, W. B. Control of automated behavior: insights from the discrete sequence production task. *Front. Hum. Neurosci.* **7**, 82 (2013).
33. Robbins, T. W. & Costa, R. M. Habits. *Curr. Biol.* **27**, R1200–R1206 (2017).
34. Watson, P. & de Wit, S. Current limits of experimental research into habits and future directions. *Curr. Opin. Behav. Sci.* **20**, 33–39 (2018).
35. Adams, C. D. & Dickinson, A. Instrumental responding following reinforcer devaluation. *Q. J. Exp. Psychol.* **33**, 109–121 (1981).
36. Dickinson, A., Nicholas, D. J. & Adams, C. D. The effect of the instrumental training contingency on susceptibility to reinforcer devaluation. *Q. J. Exp. Psychol.* **35**, 35–51 (1983).
37. Urcelay, G. P. & Jonkman, S. Delayed rewards facilitate habit formation. *J. Exp. Psychol. Anim. Learn. Cogn.* **45**, 413–421 (2019).
38. Macdonald, G. E. & de Toledo, L. Partial reinforcement effects and type of reward. *Learn. Motiv.* **5**, 288–298 (1974).
39. Shillinglaw, J. E., Everitt, I. K. & Robinson, D. L. Assessing behavioral control across reinforcer solutions on a fixed-ratio schedule of reinforcement in rats. *Alcohol* **48**, 337–344 (2014).
40. Jin, X. & Costa, R. M. Start/stop signals emerge in nigrostriatal circuits during sequence learning. *Nature* **466**, 457–462 (2010).
41. Martiros, N., Burgess, A. A. & Graybiel, A. M. Inversely active striatal projection neurons and interneurons selectively delimit useful behavioral sequences. *Curr. Biol.* **28**, 560–573 (2018).
42. Pimentel-Farfán, A. K., Báez-Cordero, A. S., Peña-Rangel, T. M. & Rueda-Orozco, P. E. Cortico-striatal circuits for bilaterally coordinated movements. *Sci. Adv.* **8**, eabk2241 (2022).
43. Erlich, J. C., Bialek, M. & Brody, C. D. A cortical substrate for memory-guided orienting in the rat. *Neuron* **72**, 330–343 (2011).
44. Turner, K. M., Svegborn, A., Langguth, M., McKenzie, C. & Robbins, T. W. Opposing roles of the dorsolateral and dorsomedial striatum in the acquisition of skilled action sequencing in rats. *J. Neurosci.* **42**, 2039–2051 (2022).
45. Tanji, J. & Shima, K. Role for supplementary motor area cells in planning several movements ahead. *Nature* **371**, 413–416 (1994).
46. Balasubramanian, S., Melendez-Calderon, A., Roby-Brami, A. & Burdet, E. On the analysis of movement smoothness. *J. Neuroeng. Rehabil.* **12**, 112 (2015).
47. Leibe, B., Matas, J., Sebe, N. & Welling, M. (eds.). *Computer Vision—ECCV 2016, Lecture Notes in Computer Science* (Springer International Publishing, 2016).
48. Mathis, A. et al. DeepLabCut: markerless pose estimation of user-defined body parts with deep learning. *Nat. Neurosci.* **21**, 1281–1289 (2018).
49. Dhawale, A. K., Smith, M. A. & Ölveczky, B. P. The role of variability in motor learning. *Annu. Rev. Neurosci.* **40**, 479–498 (2017).
50. Rueda-Orozco, P. E. & Robbe, D. The striatum multiplexes contextual and kinematic information to constrain motor habits execution. *Nat. Neurosci.* **18**, 453–460 (2015).

51. Sales-Carbonell, C. et al. No discrete start/stop signals in the dorsal striatum of mice performing a learned action. *Curr. Biol.* **28**, 3044–3055 (2018).
52. Hardwick, R. M., Forrence, A. D., Krakauer, J. W. & Haith, A. M. Time-dependent competition between goal-directed and habitual response preparation. *Nat. Hum. Behav.* **3**, 1252–1262 (2019).
53. Lehéricy, S. et al. Distinct basal ganglia territories are engaged in early and advanced motor sequence learning. *Proc. Natl Acad. Sci. USA* **102**, 12566–12571 (2005).
54. Mushiake, H. & Strick, P. L. Pallidal neuron activity during sequential arm movements. *J. Neurophysiol.* **74**, 2754–2758 (1995).
55. Menon, V., Anagnoson, R. T., Glover, G. H. & Pfefferbaum, A. Basal ganglia involvement in memory-guided movement sequencing. *Neuroreport* **11**, 3641–3645 (2000).
56. Barnes, T. D., Kubota, Y., Hu, D., Jin, D. Z. & Graybiel, A. M. Activity of striatal neurons reflects dynamic encoding and recoding of procedural memories. *Nature* **437**, 1158–1161 (2005).
57. Jog, M. S., Kubota, Y., Connolly, C. I., Hillegaart, V. & Graybiel, A. M. Building neural representations of habits. *Science* **286**, 1745–1749 (1999).
58. Andersen, K. W., Madsen, K. H. & Siebner, H. R. Discrete finger sequences are widely represented in human striatum. *Sci. Rep.* **10**, 13189 (2020).
59. Kermadi, I. & Joseph, J. P. Activity in the caudate nucleus of monkey during spatial sequencing. *J. Neurophysiol.* **74**, 911–933 (1995).
60. Markowitz, J. E. et al. The striatum organizes 3D Behavior via moment-to-moment action selection. *Cell* **174**, 44–58 (2018).
61. Jurado-Parras, M.-T. et al. The dorsal striatum energizes motor routines. *Curr. Biol.* **30**, 4362–4372 (2020).
62. Dudman, J. T. & Krakauer, J. W. The basal ganglia: from motor commands to the control of vigor. *Curr. Opin. Neurobiol.* **37**, 158–166 (2016).
63. Mello, G. B. M., Soares, S. & Paton, J. J. A scalable population code for time in the striatum. *Curr. Biol.* **25**, 1113–1122 (2015).
64. Safaie, M. et al. Turning the body into a clock: accurate timing is facilitated by simple stereotyped interactions with the environment. *Proc. Natl Acad. Sci. USA* **117**, 13084–13093 (2020).
65. Shadmehr, R., Reppert, T. R., Summerside, E. M., Yoon, T. & Ahmed, A. A. Movement vigor as a reflection of subjective economic utility. *Trends Neurosci.* **42**, 323–336 (2019).
66. Mazzoni, P., Hristova, A. & Krakauer, J. W. Why don't we move faster? Parkinson's disease, movement vigor, and implicit motivation. *J. Neurosci.* **27**, 7105–7116 (2007).
67. Ruder, L. & Arber, S. Brainstem circuits controlling action diversification. *Annu. Rev. Neurosci.* **42**, 485–504 (2019).
68. Park, J., Coddington, L. T. & Dudman, J. T. Basal ganglia circuits for action specification. *Annu. Rev. Neurosci.* **43**, 485–507 (2020).
69. Hunnicutt, B. J. et al. A comprehensive excitatory input map of the striatum reveals novel functional organization. *eLife* **5**, e19103 (2016).
70. Braun, S. & Hauber, W. The dorsomedial striatum mediates flexible choice behavior in spatial tasks. *Behav. Brain Res.* **220**, 288–293 (2011).
71. Castaño, A., Theobald, D. E. H. & Robbins, T. W. Selective lesions of the dorsomedial striatum impair serial spatial reversal learning in rats. *Behav. Brain Res.* **210**, 74–83 (2010).
72. Thorn, C. A., Atallah, H., Howe, M. & Graybiel, A. M. Differential dynamics of activity changes in dorsolateral and dorsomedial striatal loops during learning. *Neuron* **66**, 781–795 (2010).
73. Burke, D. A., Rotstein, H. G. & Alvarez, V. A. Striatal local circuitry: a new framework for lateral inhibition. *Neuron* **96**, 267–284 (2017).
74. Shadmehr, R. & Ahmed, A. A. *Vigor: Neuroeconomics of Movement Control* (MIT Press, 2020).
75. Cox, J. & Witten, I. B. Striatal circuits for reward learning and decision-making. *Nat. Rev. Neurosci.* **20**, 482–494 (2019).
76. Graybiel, A. M. The basal ganglia and chunking of action repertoires. *Neurobiol. Learn. Mem.* **70**, 119–136 (1998).
77. Carelli, R. M., Wolske, M. & West, M. O. Loss of lever press-related firing of rat striatal forelimb neurons after repeated sessions in a lever pressing task. *J. Neurosci.* **17**, 1804–1814 (1997).
78. Ashe, J., Lungu, O. V., Basford, A. T. & Lu, X. Cortical control of motor sequences. *Curr. Opin. Neurobiol.* **16**, 213–221 (2006).

**Publisher's note** Springer Nature remains neutral with regard to jurisdictional claims in published maps and institutional affiliations.

Springer Nature or its licensor (e.g. a society or other partner) holds exclusive rights to this article under a publishing agreement with the author(s) or other rightsholder(s); author self-archiving of the accepted manuscript version of this article is solely governed by the terms of such publishing agreement and applicable law.

© The Author(s), under exclusive licence to Springer Nature America, Inc. 2023

## Methods

### Animals

The care and experimental manipulation of all animals were reviewed and approved by the Harvard Institutional Animal Care and Use Committee. Experimental participants were female Long Evans (strain code 006) rats 3–8 months old at the start of training (Charles River, RRID: RGD\_2308852).

### Statistics and reproducibility

Because the behavioral effects of our circuit manipulations could not be prespecified before the experiments, we chose sample sizes that would allow for the identification of outliers and for validation of experimental reproducibility. Animals were excluded from experiments post hoc if the lesions were found to be outside the intended target area or affected additional brain structures ('Lesion Surgeries' and 'Histology'). Additionally, units with very low firing rates (<0.25 Hz) or units not recorded across all trial types during task execution were excluded from analyses (see 'Criteria for Unit Selection' for details). The investigators were not blinded to allocation during experiments and outcome assessment, unless otherwise stated.

Statistical tests applied to the behavioral data were nonparametric and did not assume normality. Statistical tests applied to electrophysiological data used parametric statistical tests (Student's *t* test). The data distribution for these analyses was assumed to be normal, but this was not formally tested. All statistical tests were two-sided. For more details and a description of the test used for each figure, see Supplementary Table 1.

No statistical methods were used to predetermine the number of participants in our study, but our sample sizes were similar to those reported in previous publications<sup>15,40,44,50</sup>. The participants were randomly allocated to experimental groups. Data collection and analyses were not performed blind to the conditions of the experiments, except for histological verification of lesion location and sizes.

### Behavioral apparatus

Animals ( $n = 23$  total) were trained on our discrete sequence production task (the 'piano' task) in a fully automated home-cage training system<sup>79</sup>. Hardware was controlled by Teensy 3.6, and experiments and videos were recorded by Raspberry Pi 3. Home-cage training was done in custom-made behavioral boxes. Boxes were outfitted with three levers spaced ~2.5 cm apart and 14 cm above the floor. Plastic barriers 0.25' thick, 2.3' tall and of 1' extent were placed between each lever to restrict the postures with which a rat can use their forelimb to press levers. A reward spout for water delivery was placed beneath the center lever. Lever presses were registered when lever displacement reached a threshold, corresponding to an angular deviation from the horizontal of -14 degrees. Lever displacements were measured by optical sensors (Digi-Key, QRE1113-ND). Three cameras (Raspberry Pi Camera Module V2) recorded videos from each side of the box and from the top (Extended Data Figs. 2a and 6a).

### Behavioral training

Water-deprived rats received four 40-min training sessions during their subjective night, spaced 2 h apart. Starts of sessions were indicated by blinking house lights, a continuous 1 kHz pure tone, and a few drops of water. At the end of each night, water was dispensed freely up to the daily minimum (5 ml per 100 g body weight).

Notably, we wanted our paradigm to distinguish motor automaticity from habit formation<sup>59</sup>, two independent processes that can occur alongside each other and that may involve some of the same neural substrates<sup>5,33,80</sup>. Thus, we designed our task to ensure that rats achieve automaticity on a motor sequence without developing it into a habit. Because habits tend to form when the correlation between actions and outcomes is weak or variable<sup>35,36,81</sup>, if the reward is delayed<sup>37</sup>, or,

further, if the reward is appetitive or addictive<sup>38,39,82</sup>, our paradigm directly linked behavioral variants to a water reward in a training process<sup>36</sup> that resulted in highly overtrained behaviors expressed in goal-directed ways.

### Stages of training.

1. Rats were initially pretrained to associate a visual cue with a lever press. On each trial, one of three LEDs above each of the three levers, chosen randomly, would light up to signify the 'correct' lever. Correct presses were rewarded while incorrect presses triggered a 1.2-s time-out, which was retriggered for every press in the time-out period. To prevent rats from only selecting a single lever, we gradually decreased the probability of cueing a repeatedly pressed lever. All rats ( $n = 18$ ) learned to associate levers with cues in a median of 5,284 trials. The criterion for learning was performing at >90% success rate for >100 trials.
2. After learning to associate visual cues with levers, rats were rewarded only when performing consecutive lever presses. Initially, rewards were provided for every two successful consecutive presses, but after 500 rewards, reward was dispensed only after every three consecutive lever presses. Cued levers were constrained to not repeat, giving 12 different possible three-lever sequences. Rats quickly learned to press levers in a sequence and no longer visited the reward port in between consecutive presses.
3. Following 1,000 successful three-lever trials, rats were introduced to the block structure (Fig. 2a), which was modeled on a sequence task in primates<sup>45</sup>. In the block structure, the same three-lever sequence is cued on each trial until there are six successful performances, and then a new sequence is randomly chosen. Cues are presented sequentially with no delay.
4. After ~1–2 weeks of training on the block structure, WM trials were introduced by withholding the second and third cued lever in the 4th–6th trial of the block. Missed uncued levers were not required to be repeated until successful for a new sequence to be chosen.
5. One of the four nightly flexible sessions was changed to an automatic session. In this session, rats were required to perform only a single three-lever sequence, chosen randomly for each rat. This sequence was initially fully cued. Cues were then removed in reverse sequence, from the last lever to the first lever, every time the rat performed at >50% success rate over 30 trials. If the success rate fell below 20% for 30 trials, or if rats failed to press the lever once in the entire session, a cue would be added back in. All rats were able to perform >100 trials with at least two of the three cues withheld after  $1,024 \pm 438$  (mean  $\pm$  s.e.m.) trials or  $17 \pm 10$  (mean  $\pm$  s.e.m.) days. After learning the sequence without cues, they would occasionally ( $5.18\% \pm 1.39\%$  (s.e.m.) of trials) hit the lower threshold prompting the addition of cues.

### Behavior analysis

In total, 23 rats were trained on the three-lever task. In total, 12 of 23 rats were used to characterize the behavior; nine rats were excluded because kinematics was not captured or analyzed early in training.

**Definition of expert performance.** Expert performance was determined when success rates and trial times stabilized to within 0.5% of final performance values (based on the last 2,000 trials). Metrics (success rates and trial time) were smoothed with a moving average of 400 trials. Furthermore, we required automatic performance to reach >72% success rates to be considered 'expert,' following previous studies<sup>50,57,72,83</sup>.

**Calculation of performance metrics.** Success rate. The success rate is defined as the number of rewarded trials divided by the total number of attempted trials.

**Trial time.** Trial time is defined as the interval between the first and third lever press. This only includes successful sequences, as incorrect sequences may not include three full lever presses.

**Error variability.** Error variability is defined as the Shannon entropy (in bits) of the probability of each sequence occurring for a given target sequence. Low probability sequences ( $P < 0.001$ ) are discarded. If mistakes are systematic, the probability distributions will be skewed toward particular erroneous sequences, and the entropy will be low. If mistakes are made randomly, the distribution will look more uniform, and the entropy will be high. For flexible sequences, the error calculation was done on the sequence chosen for the AUTO task.

**Error modes.** Motor errors are defined as failures to touch or fully depress the ‘correct’ lever in what would otherwise have been a correct sequence (Supplementary Video 2). That is, the rat oriented to the ‘correct’ lever and swiped at it but failed to depress it beyond the threshold for detection. Sequence errors, on the other hand, involved orienting to and pressing the wrong lever. For each rat and session type (flexible and automatic), ~100 videos of error trials were manually inspected and labeled as either a sequence or motor error. To analyze behavior following different error mode types (Fig. 3f), we used a heuristic to automatically estimate and classify failures as motor or sequence errors. This allowed us to analyze >100 trials. In this analysis, motor errors were classified as any error sequence that resembled an omitted lever (for example, for the target sequence, LRC, RC and LC are considered motor errors), while sequence errors are any other type of mistake. This heuristic generally overestimates motor errors ( $29.65\% \pm 5.9\%$  of errors for CUE trials,  $16.95\% \pm 5.48\%$  of errors for WM trials,  $13.16\% \pm 5.32\%$  of errors for AUTO trials, data is mean  $\pm$  s.e.m.) and underestimates sequence error. Trial-dependent accuracies and trial times, conditioned on the type of trial that came before (hit, motor error, sequence error), were then calculated using this heuristic (Fig. 3f). For trial times, we only considered sequences that had the same overall movement length as the overtrained sequence (because L→R is further to travel than L→C) as a control.

**Average forelimb speed.** Raw trajectories (position traces) of the active forelimb were smoothed and upsampled (from 40 Hz to 120 Hz) using cubic smoothing spline (csaps in Matlab, smoothing parameter of 0.1). Instantaneous velocities for the horizontal (x) and vertical (y) positions were calculated and then converted to instantaneous speed. This value was averaged from 0.1 s before the first lever press to 0.1 s after the last one. Because velocity was calculated from a side-view camera and animals moved toward and away from the camera to press different levers, we left velocity measures in pixels per second.

**Movement smoothness.** To quantify the smoothness of the movement, or its continuity and nonintermittency<sup>46</sup>, we measured each trajectories spectral arc length, a dimensionless metric that measures the arc length of the Fourier magnitude spectrum within an adaptive frequency range<sup>84</sup>. This metric quantifies smoothness independent of amplitude and duration and is less sensitive to noise than another popular smoothness metric, the log-dimensionless jerk<sup>46</sup>. Values are scaled between the maximum and minimum average spectral arc length recorded across rats in Figs. 2i, 6i and 7i. Values closer to 1 are more smooth.

**Trial selection for behavioral analysis.** In Fig. 2, early performance is taken from the first 1,000 trials and late performance is measured from the last 1,000 trials. For Fig. 3, metrics are calculated from all trials after

the expert performance was reached. For Figs. 6 and 7, prelesion and postlesion accuracies are calculated from the week before and after the lesion. Prelesion and postlesion trial times, trial speeds and kinematics are taken from the last 1,000 trials before and after the lesion. Finally, it is important to note that because automatic sessions are introduced after the flexible sessions, early performance on automatic (AUTO) trials benefits from prior flexible practice (Fig. 2).

**Kinematic tracking.** To track the movements of the rat’s active forelimb and head during our task, we used recent machine-learning approaches to detect keypoints from individual video frames. Videos of animals performing the task were acquired at 40 Hz (90 Hz for DLS recording cohort) from cameras pointing at the lever from the two sides to obtain both forelimb trajectories and one camera pointing down from the top to obtain the rat’s horizontal position. For video-based tracking, we trained ResNet-50 networks pretrained on ImageNet, using DeeperCut (<https://github.com/eldar/pose-tensorflow>)<sup>47</sup>. To refine the tracking for our rats, we randomly selected about ~200 frames per view and trained the network using manually labeled position of the hand and nose. The network was then used to predict the position of body parts across all trials on a frame-by-frame basis, using graphics processing units in the Harvard Research Computing cluster. Tracking accuracy was qualitatively validated post hoc by visual inspection of five trials across three different sessions. Frames with poor tracking (<0.95 score from the model), due to occlusion of the forelimbs, were removed, and trajectories in those frames were linearly interpolated. If >5 consecutive frames were removed, the trial was discarded for tracking purposes. Additionally, any trial with >5% of poorly tracked frames was removed from the analysis. The full trial trajectory was then smoothed using a Gaussian filter in MATLAB, with a  $\sigma$  of 0.6 frames.

To track the movements of the rat’s active forelimb and nose in three dimensions, we first calibrated our multiple camera views (left side, right side, top side; Extended Data Fig. 6a) to a set of manually labeled features in our box observable from both views to calculate camera extrinsics and world coordinates, drawing from camera calibration functions in the Computer Vision Toolbox (for example, estimateWorldCameraPose, estimateCameraParameters, cameraPoseToExtrinsics). We could then use the calibrated cameras to triangulate our 2D estimated points into 3D<sup>85</sup>. For the forelimb, we triangulated from 2D points tracked on the left and right cameras (Extended Data Fig. 6b). The nose used either the left and top or right and top cameras. 3D world coordinates are in millimeters, relative to one of the manually labeled features in the box.

**Kinematic analyses.** To quantitatively compare kinematic similarity, we computed pairwise trial-to-trial correlations. Because trial times varied, movement trajectories were time-warped to a common template. Specifically, trajectories from each trial were interpolated so that the time between the first and second lever and the time between the second and third lever matched the median interlever intervals. For submovement correlations, trajectories are warped to the median interlever interval time. Although we tracked both forelimbs, analyses were performed only on the active forelimb used to press the lever. Rats used a single forelimb to perform lever presses ( $n = 12/23$  right and  $n = 11/23$  left).

### Electrophysiological recordings

Microdrive construction, surgical and recording procedures were performed as previously described<sup>86</sup>. After expert performance was reached on the sensory-guided, memory-guided and automatic tasks, a microdrive containing arrays of 16 tetrodes was implanted into the DLS ( $n = 4$  rats) contralaterally to the active forelimbs as previously described<sup>15</sup> (Extended Data Fig. 3a). We first made a 4–5 mm diameter craniotomy and removed the dura, before lowering the 16 tetrode array to the DLS (see Supplementary Table 2 for coordinates). Neural and

behavioral data were recorded continuously for  $95 \pm 31$  d. The drive was occasionally advanced by  $\sim 200$   $\mu\text{m}$ , 0–4 times over the course of the experiment. At the end of the experiment, an electrolytic lesion was done to mark the electrode site. This was done by passing a  $30$   $\mu\text{A}$  anodal current for 15 s through the electrode tips. For implant coordinates, according to ref. 87, see Supplementary Table 2.

### Lesion surgeries

After reaching expert performance, bilateral striatal lesions were performed ( $n = 7$  DLS,  $n = 6$  DMS; for full details, see refs. 15,16). For injection coordinates, see Supplementary Table 2. Anesthetized animals (2% isoflurane in carbogen) were placed in a stereotactic frame. Bregma was located after incision along the midline, and small craniotomies were performed above the targeted brain areas. Quinolinic acid (Sigma-Aldrich; 0.09 M in PBS (pH 7.3)) was injected in 4.5 nl increments, via a thin glass pipette connected to a microinjector (Nanoject III; Drummond). Lesions were performed in two stages, starting with the side contralateral to the primary forelimb (the forelimb that presses the first lever). Animals recovered for 7 d minimum before being reintroduced to training.

### Histology

At the end of the experiment, animals were killed ( $100$  mg  $\text{kg}^{-1}$  ketamine and  $10$  mg  $\text{kg}^{-1}$  xylazine), transcardially perfused with either 4% paraformaldehyde (PFA; for nissl staining to confirm lesion size and location) or 2% PFA and 2.5% glutaraldehyde (for osmium staining, to confirm location of electrode implant) in 1× PBS. For electrode implants, brains were then stained with osmium (as described in ref. 88) and embedded in epoxy resin for micro-computed tomography (CT) scanning. Micro-CT scans (X-Tek HMS ST 225; Nikon Metrology) were taken at 130 kV, 135 uA with 0.1 mm copper filter and a molybdenum source. 3D volume stacks were reconstructed (VGStudio MAX), and brains were aligned along the coronal, medial and sagittal planes using Fiji. Location of the electrolytic lesion could be calculated relative to anatomical landmarks (that is, corpus callosum split at anterior/posterior = 1.65 mm from bregma, anterior commissure split at 0 mm bregma). For lesioned animals, brains were sectioned into 80- $\mu\text{m}$  slices using a Vibratome (Leica) and then mounted and stained with cresyl violet. Images of whole brain slices were acquired at  $\times 10$  magnification with either a either a VS210 whole slide scanner (Olympus) or an Axioscan slide scanner (Zeiss). To quantify the extent and location of striatal lesions, we analyzed coronal sections spanning the anterior-posterior extent of the striatum from four calibration animals and two experimental animals (DLS) (seven hemispheres injected in total) or from four experimental animals (DMS). Boundaries were manually marked based on differences in cell morphology and density<sup>89</sup>. The extent of the striatum was defined based on the Paxinos and Watson rat brain atlas<sup>87</sup>, using anatomical landmarks (external capsule and ventricle) and cell morphology and density.

### Neural analysis

**Spike sorting.** Raw neural data were collected continuously over the course of the experiment (mean and s.e.m. are  $95 \pm 31$  d,  $n = 4$  fully trained rats). Spiking activity from populations of single units was sorted using our custom-designed spike-sorting algorithm, fast automated spike tracker (FAST)<sup>86</sup>. A custom MATLAB graphical user interface (<https://github.com/Olveczky-Lab/FAST-ChainViewer>) was used to manually isolate and track single units over long timescales. On average, we isolated  $20.5 \pm 13.3$  units simultaneously in the striatum within each session. We were able to track units for an average of  $4.3 \pm 1.2$  d. Assessing the quality of sorted single unit was done as previously described<sup>86</sup>.

**Unit type identification.** Units were identified as putative MSNs or FSIs based on their peak width (full width at half maximum) and time

interval between spike peak and valley<sup>90</sup>. Units with peak width  $>150$   $\mu\text{s}$  and peak-valley interval  $>500$   $\mu\text{s}$  were classified as MSNs, while units with peak width  $\leq 150$   $\mu\text{s}$  and peak-valley interval  $\leq 500$   $\mu\text{s}$  were classified as FSIs.

**Criteria for unit selection.** We selected a subset of the total population of recorded units for our neural analyses. To be included, we required that a neuron fired at least 1 spike, on at least 25% of all trials and was recorded over  $>5$  rewarded trials in each task condition (CUE, WM and AUTO) for Fig. 4, or  $>5$  rewarded trials in each of the 12 different sequences. From a total of 2,468 recorded and well-isolated units, this criterion reduced the units available for analysis to 579 units for the comparison across task conditions and to 340 units for comparisons across sequences in the flexible sessions.

**Neural metrics.** Trial-averaged, z-scored activity. First, instantaneous firing rates were calculated for each trial by convolving binned (10 ms bins) spike counts with a Gaussian kernel ( $\sigma = 25$  ms). To account for differences in trial times, firing rates were then local linearly warped to the median press times. Warping was done only after calculating firing rates to not artificially increase or decrease the firing rate. Firing rates before the first and after the last lever press were not warped. After this alignment step, each trial was z-scored and then averaged over for each unit and each task condition.

**Average firing rates.** Firing rates on individual trials were calculated from  $-0.2$  s before the first lever press to  $0.2$  s after the third lever press. This value was averaged over every trial for a given task condition.

**Average activity.** To determine if there was elevated population activity at privileged time points in the sequence of the task (for example, at the boundaries of discrete motor elements), we averaged over the time-varying z-scored activity for each unit recorded in a rat. This average trace was compared to a distribution of average z-scored activity, sampled from random times in the behavior (2 s before and after the first and last lever press,  $n = 1 \times 10^4$  permutations).

**Correlation across task conditions.** For each unit, correlation coefficients were computed between the time-varying vector of trial-averaged activity across task conditions.

**Correlating neural activity associated with behavioral elements across sequences.** We computed the correlations between neural population vectors of combined orienting and lever-pressing movements across the 12 different sequences. Population vectors were calculated by averaging the activity of each neuron over orienting and lever-press movements. Orienting movements were defined as those that occurred 0.1 s after a prior lever press until 0.1 s before the next press. Lever-press movements were defined as occurring  $\pm 0.1$  s around the lever deflection. We excluded the first lever press for this analysis, as it was not preceded by an orienting movement.

**Principal components (PCs).** PC analysis was performed on the matrices of population activity (neurons versus time) concatenated across either the three task conditions (CUE, WM and AUTO) or the 12 sequences along the time dimension. Task conditions or sequences were then disjoined to generate the plots in Figs. 4e and 5d.

**Neural decoding analysis.** We used a feed-forward neural network with two hidden layers to predict the time-varying, 2D velocity components of the active forelimb (side camera) and the nose (top camera) from the spiking activity of ensembles of DLS neurons. Spiking activity was binned in 25 ms bins. We used 75 ms of coincident spiking activity as the input to the model. Other model parameters were the same as in previous work<sup>15</sup>. We additionally challenged our network to predict

the 3D velocity components of the active forelimb and nose, from 3D world coordinates triangulated from calibrated cameras (described above; Extended Data Fig. 6d–f).

We trained our models on blocks of >50 trials in which there were at least 12 simultaneously recorded units that had an average firing rate of >0.25 Hz during the trials. In each block of trials, we fit decoding models using the activity of up to  $n = 20$  randomly sampled ensembles of 12 striatal units. We quantified model performance using twofold cross-validation by computing the pseudo- $R^2$ : pseudo- $R^2 = 1 - \frac{\sum(X - \hat{X})^2}{\sum(X - \bar{X})^2}$ .

Decoding performance (pseudo- $R^2$ ) was measured in each ensemble, averaged across all 20 ensembles and then averaged across all blocks of trials for each rat. For the subset model, the training dataset was generated from only six of the 12 sequences, chosen at random for each of the  $n = 20$  ensembles. The test dataset was then generated from the remaining six sequences.

### Neural network model

We simulated an artificial neural network consisting of two populations, one corresponding to DLS and another to other downstream motor circuits. The DLS network contained no recurrent connections, while the downstream network contained all-to-all recurrent weights. The two populations were bidirectionally connected with all-to-all feed-forward and feedback weights. The downstream motor network directly controls movement via a set of feed-forward weights and also receives an additional source of input representing cue signals via a set of feed-forward weights. Each network consists of 500 units with a rectified linear (ReLU) activation function. Network weights were initialized with the Kaiming uniform initialization<sup>91</sup>. Gaussian noise of s.d. 0.1 was added to the inputs to each neuron in both networks at every timestep in all simulations.

We modeled a simplified version of the experimental task in which the output of the network controls the velocity of a ‘forelimb’ (represented simply as a point) and is tasked with moving it into a set of three circular target zones in a prescribed sequential order, as in the piano task. The target zones were positioned as shown in Fig. 8b. On each trial, the loss function measuring the performance of the network was defined as the sum of the squared distance between the forelimb position and the center of the current target. The identity of the current target changes to the next in the sequence once it is reached. On cued trials, the target lever changed, and on the first step, cue input was provided to the downstream network in the form of a vector indicating the position of the cue relative to the forelimb. The cue input was transient, lasting only one timestep for each cue. If the sequence was not performed successfully within  $T = 40$  timesteps of the simulation, the trial was halted and considered a failure.

The network, excluding the DLS input and output weights, was pretrained on the cued task for 100,000 iterations (well past the point where asymptotic performance was reached). The DLS input weights were then trained on randomly interleaved cued and automatic task trials (50% probability of each, with all 12 possible target trajectories equally likely on cued trials), again for 100,000 iterations. The target sequence on automatic trials was always the same (right, center and left). All network training used backpropagation and the Adam optimizer with a learning rate set to  $1 \times 10^{-4}$ . The training was conducted using PyTorch.

In Extended Data Fig. 10a–g, we modified the network architecture by replacing the NxN DLS output weights with a chain of Nx1 and 1xN weights, corresponding to a rank-1 projection. In Extended Data Fig. 10h–m, we modulated the gain of DLS activity, suppressing it by a factor of 0.1 at all timesteps except the first and those when the target lever changed. In Extended Data Fig. 10n–s, we omitted the pretraining stage and instead trained the entire model on all task conditions for 200,000 iterations.

### Reporting summary

Further information on research design is available in the Nature Portfolio Reporting Summary linked to this article.

### Data availability

The generated datasets are available from the corresponding author upon reasonable request.

For databases/datasets used in tracking, see <https://pose.mpi-inf.mpg.de/#related>.

### Code availability

All MATLAB analysis scripts will be made available upon reasonable request.

Movement smoothness implementations: <https://github.com/siva82kb/smoothness/tree/master/matlab>

DeeperCut Implementation: <https://github.com/eldar/pose-tensorflow>

Spike sorting (FAST) implementation: <https://github.com/Olveczky-Lab/FAST-ChainViewer>

### References

79. Poddar, R., Kawai, R. & Ölveczky, B. P. A fully automated high-throughput training system for rodents. *PLoS ONE* **8**, e83171 (2013).
80. Kondapavulur, S. et al. Transition from predictable to variable motor cortex and striatal ensemble patterning during behavioral exploration. *Nat. Commun.* **13**, 2450 (2022).
81. Derusso, A. L. et al. Instrumental uncertainty as a determinant of behavior under interval schedules of reinforcement. *Front. Integr. Neurosci.* **4**, 17 (2010).
82. Vandaele, Y., Pribut, H. J. & Janak, P. H. Lever insertion as a salient stimulus promoting insensitivity to outcome devaluation. *Front. Integr. Neurosci.* **11**, 23 (2017).
83. Guo, J.-Z. et al. Cortex commands the performance of skilled movement. *eLife* **4**, e10774 (2015).
84. Beck, Y. et al. SPARC: a new approach to quantifying gait smoothness in patients with Parkinson’s disease. *J. Neuroeng. Rehabil.* **15**, 49 (2018).
85. Hartley, R. & Zisserman, A. *Multiple View Geometry in Computer Vision* (Cambridge University Press, 2003).
86. Dhawale, A. K. et al. Automated long-term recording and analysis of neural activity in behaving animals. *eLife* **6**, e27702 (2017).
87. Paxinos, G. *The Rat Brain in Stereotaxic Coordinates* (Academic Press, 1998).
88. Masis, J. et al. A micro-CT-based method for quantitative brain lesion characterization and electrode localization. *Sci. Rep.* **8**, 5184 (2018).
89. Feng, Q. et al. Specific reactions of different striatal neuron types in morphology induced by quinolinic acid in Rats. *PLoS ONE* **9**, e91512 (2014).
90. Berke, J. D., Okatan, M., Skurski, J. & Eichenbaum, H. B. Oscillatory entrainment of striatal neurons in freely moving rats. *Neuron* **43**, 883–896 (2004).
91. He, K., Zhang, X., Ren, S. & Sun, J. Delving Deep into rectifiers: surpassing human-level performance on ImageNet classification. in *Proceedings of the IEEE International Conference on Computer Vision (ICCV)* 1026–1034 (IEEE, 2015).

### Acknowledgements

We thank K. Hardcastle, N. K. Harpaz, K. Laboy-Juarez, D. Aldarondo and P. Zmarz for their helpful discussions and comments on the manuscript. We also thank S. Iuleu, M. Shah and G. Pho for technical support, D. Aldarondo for help with 3D tracking, in addition to S. Turney and the Harvard Center for Biological Imaging, as well as G. Lin and the Harvard Center for Nanoscale Systems for infrastructure and

support. S. Wolff, A. Dhawale and J. Marshall provided experimental advice and helped in analyzing and interpreting the data. This work was supported by National Institutes of Health (NIH) (grants R01-NS099323 (B.P.Ö.) and R01-NS105349 (B.P.Ö. and G.S.E.)). J.L. was also supported by the Department of Energy's Computational Science Graduate Fellowship (DOE CSGF) (DE-SC0020347). The funders had no role in study design, data collection and analysis, decision to publish or preparation of the manuscript.

## Author contributions

K.G.C.M. and B.P.Ö. conceived and designed the study. K.G.C.M. conducted the experiments and analyzed the data. J.L. and G.S.E. designed and analyzed the model. K.G.C.M. and B.P.Ö. wrote the manuscript with critical input from J.L. and G.S.E.

## Competing interests

The authors declare no competing interests.

## Additional information

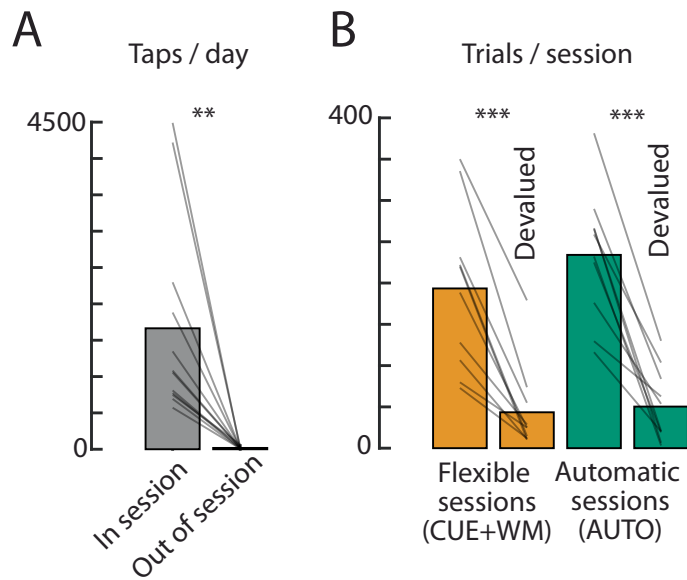
**Extended data** is available for this paper at  
<https://doi.org/10.1038/s41593-023-01431-3>.

**Supplementary information** The online version contains supplementary material available at  
<https://doi.org/10.1038/s41593-023-01431-3>.

**Correspondence and requests for materials** should be addressed to Bence P. Ölveczky.

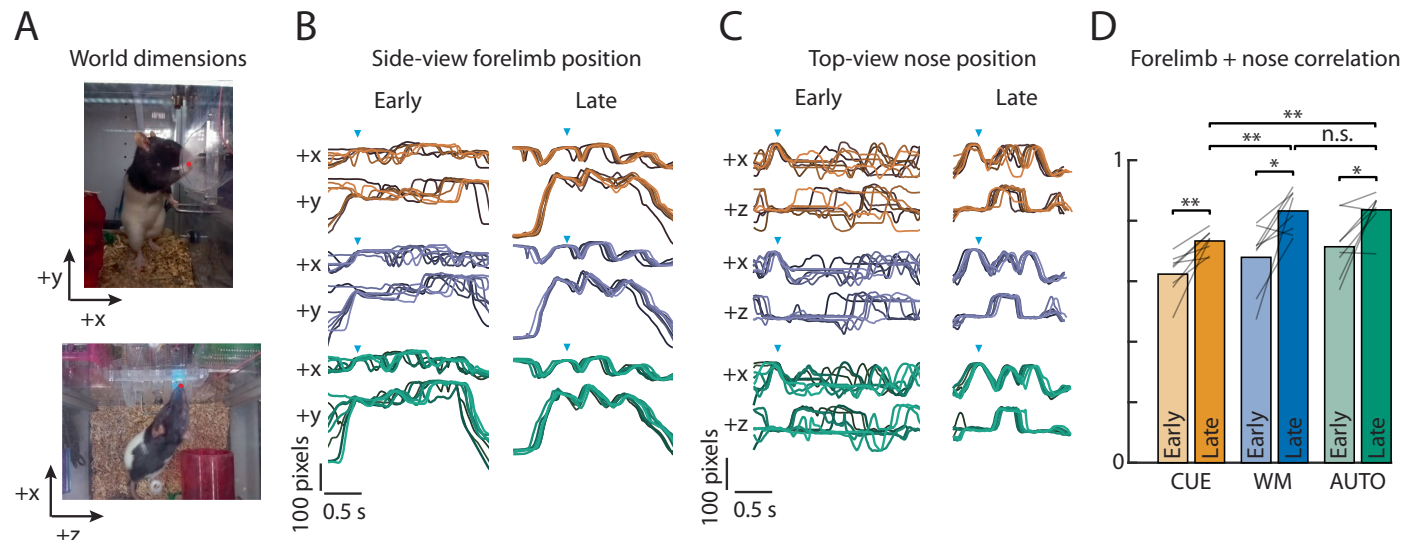
**Peer review information** *Nature Neuroscience* thanks David Robbe and the other, anonymous, reviewer(s) for their contribution to the peer review of this work.

**Reprints and permissions information** is available at  
[www.nature.com/reprints](http://www.nature.com/reprints).



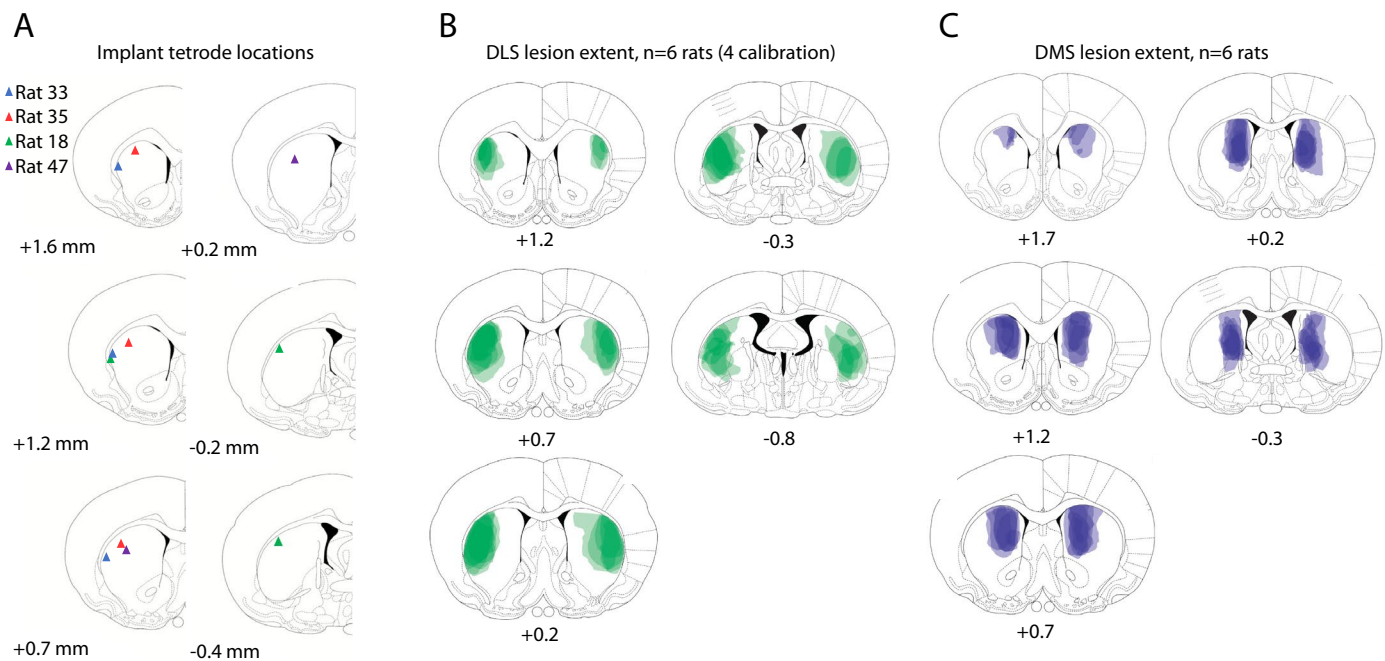
**Extended Data Fig. 1 | Rats express flexible and automatic behaviors in a goal-directed way.** **a.** Average number of taps performed per day. Homecage trained rats engage with the levers, which are always present, only during session times ( $n = 12$  rats). **b.** Average number of trials per session, plotted for flexible

(orange) and automatic (automatic) sessions, for typical and devalued sessions (see Methods,  $n = 10$  rats). Bars indicate the grand average across rats, and lines are individual rats. \*\* $P < 0.01$ , \*\*\* $P < 0.001$ , two-sided t-test.



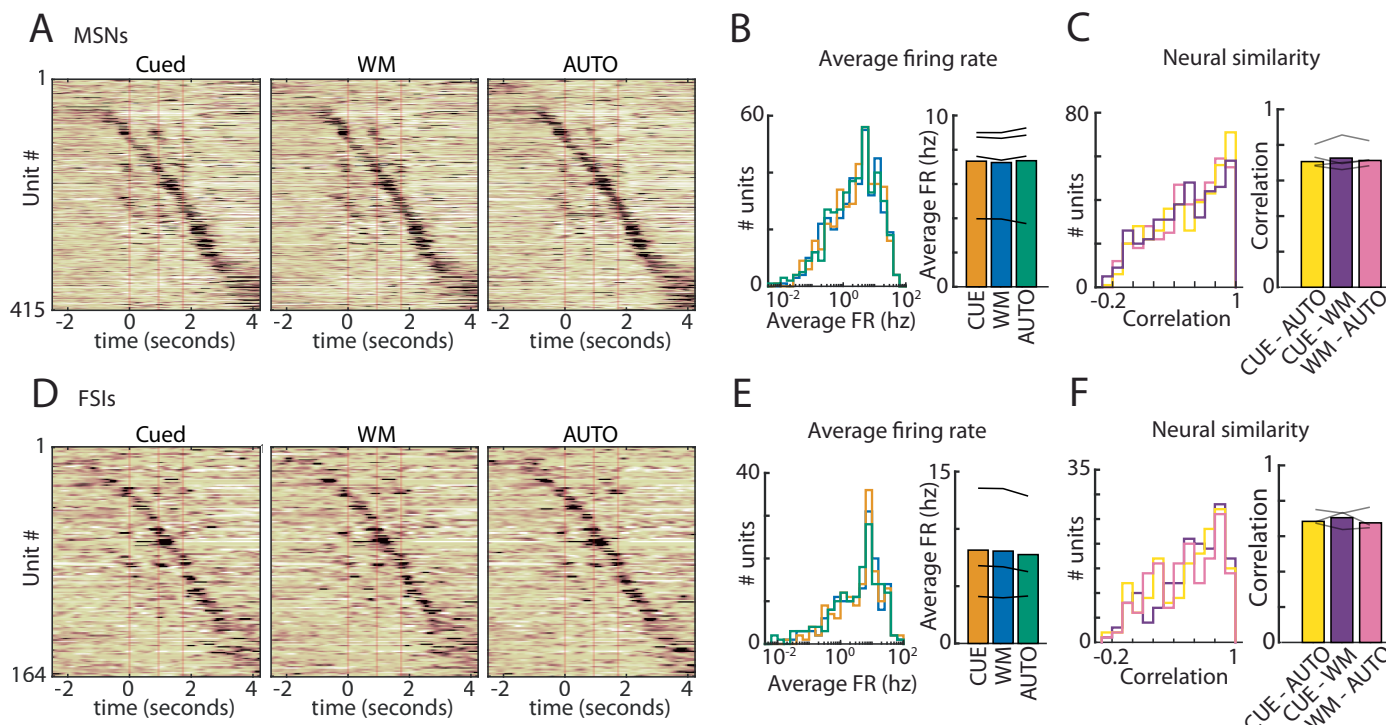
**Extended Data Fig. 2 | Rat's movements increase stereotypy along other axes and joints.** **a.** View of 'piano task' from a side (right) and top camera. Axes are defined as +x – towards lever, +y – towards top of box, and +z – towards right lever along the piano. **b.** Replotted from Fig. 1e is 8 example forelimb trajectories in the x and y dimension for each task condition from early and late in learning. Orange

– CUE, blue – WM, green – AUTO. **c.** Same as B., but for the nose position in the x and z dimension. **d.** The average, trial-to-trial correlation of forelimb (in x and y dimensions) and nose (in x and z dimensions) trajectories increases with training. Bars represent grand averages over rats, and lines are averages within individual rats ( $n = 8$  rats). \* $P < 0.05$ , \*\* $P < 0.01$ , Wilcoxon two-sided sign-rank test.



**Extended Data Fig. 3 | Histology of DLS implants, DLS lesions, and DMS lesions.** **a.** Location of recording electrode implantation sites in DLS marked with a colored arrowhead for each of the 4 rats. For some individuals multiple sites are marked, due to individual tetrode bundles spreading during implantation. Coronal slices are labeled from distance relative to bregma. **b.** The extents of DLS lesions from 6 rats (11 hemispheres) are marked for the DLS lesion along the

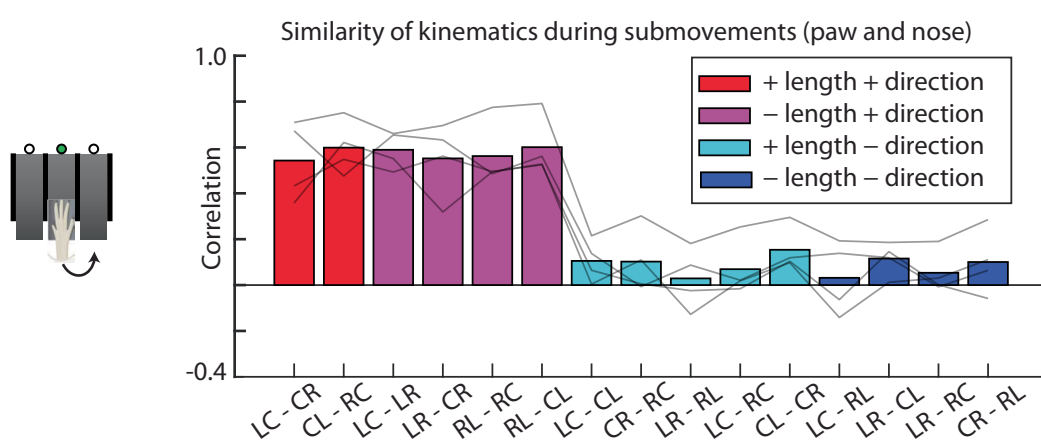
anterior-posterior axis of the striatum, and shaded in green. Lesion extent was calibrated to target the motor cortex-recipient region of dorsolateral striatum, as determined from virally-mediated fluorescent labeling in<sup>24</sup>. **c.** Same as B, but 12 across 6 rats hemispheres are labeled for DMS lesions. Targeting is based on the prefrontal cortex recipient region of dorsomedial striatum, also from work in<sup>24</sup>.



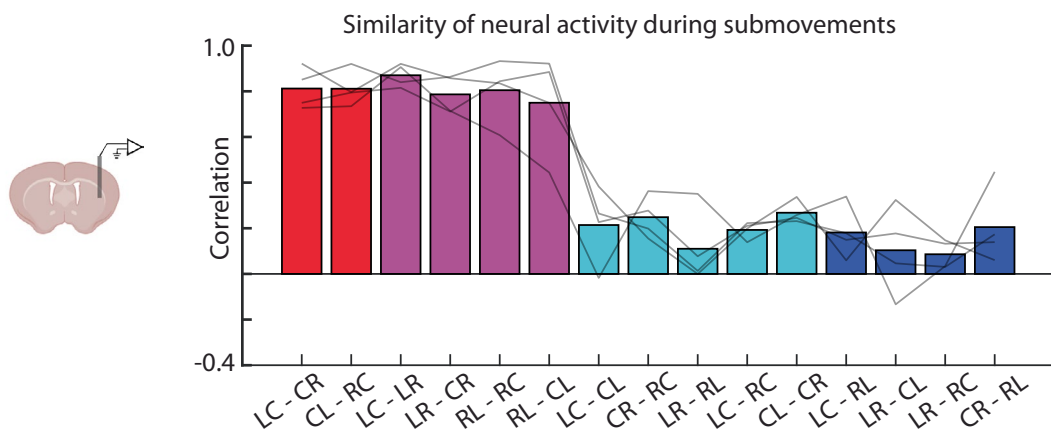
**Extended Data Fig. 4 | MSNs and FSIs represent AUTO, CUE, and WM sequences similarly.** **a.** Z-scored average activity of 415 putative medium spiny neurons (MSNs) recorded in the DLS for the same sequence during the AUTO, CUE, and WM task condition (from  $n = 4$  rats). The trials were linearly time-warped to each lever press (red vertical lines). Units were sorted by the time of their peak activity. The sorting index was calculated from half the available trials for each unit, taken from the AUTO task, and then applied to the remaining trials and tasks. **b.** (Left) Histogram of the average firing rate of putative MSNs during the trial period for each task condition. (Right) Average firing rates across all

rats are not significantly different ( $p > 0.05$ , two-tailed t-test). Lines represent individual rats. **c.** (Left) Histogram of correlation coefficients of trial-averaged neural activity across the task conditions (CUE x WM - purple, WM x AUTO - pink, CUE x AUTO - yellow). (Right) Average correlation coefficient across all units, for each rat ( $n = 4$ ). Average correlations are not significantly different across each task comparison ( $p > 0.05$ , two-tailed t-test). **d-f.** Same as A-C, but for 164 putative FSIs. Note  $n = 3$  only, as one rat had no putative FSIs recorded that met our criteria (see Methods).

A

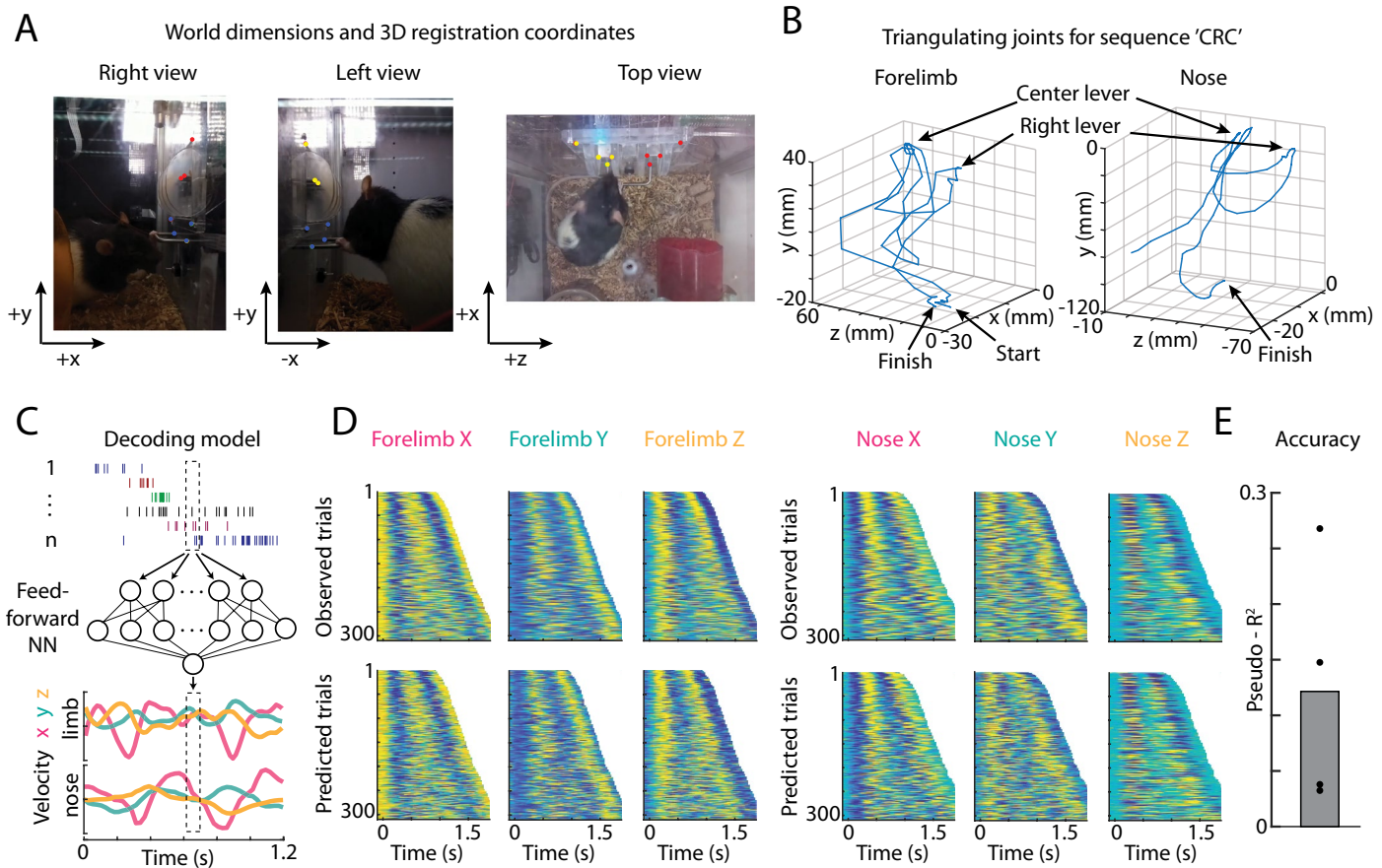


B



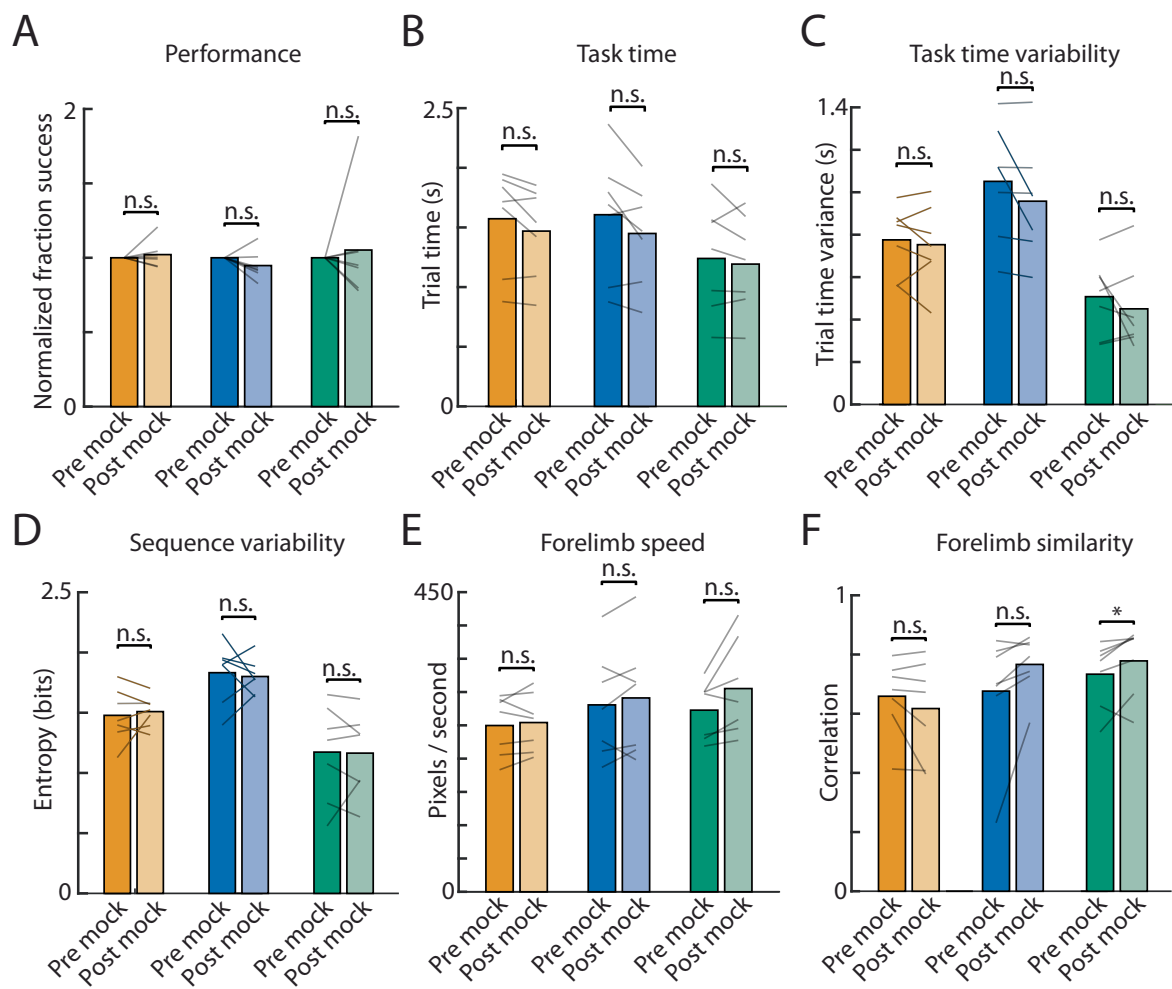
**Extended Data Fig. 5 | Neural and kinematic similarity for all orientation movements.** **a.** Comparing kinematic similarity across different orientation movements. Plotted is the average trial-to-trial correlation between kinematic traces of the forelimb (side view, x and y) and nose (top view, x and z) from different orientation movements (for example, L > C and C > R). Orientation movements are cropped 0.2 seconds after and before the lever presses. Bars are averages across rats, and lines represent averages in individual rats ( $n = 4$ ). Colors

denote whether orientation movements match in length (that is short vs. long) or orientation direction (that is left- vs. right-wards). **b.** Comparing neural similarity across different orientation movements. Bars indicate average similarity across all rats, lines denote individual rats ( $n = 4$ ). Population activity is averaged during the orientation movement (defined as 0.2 seconds after and before the presses) for each different orientation movement, and correlation coefficients are computed between population vectors.



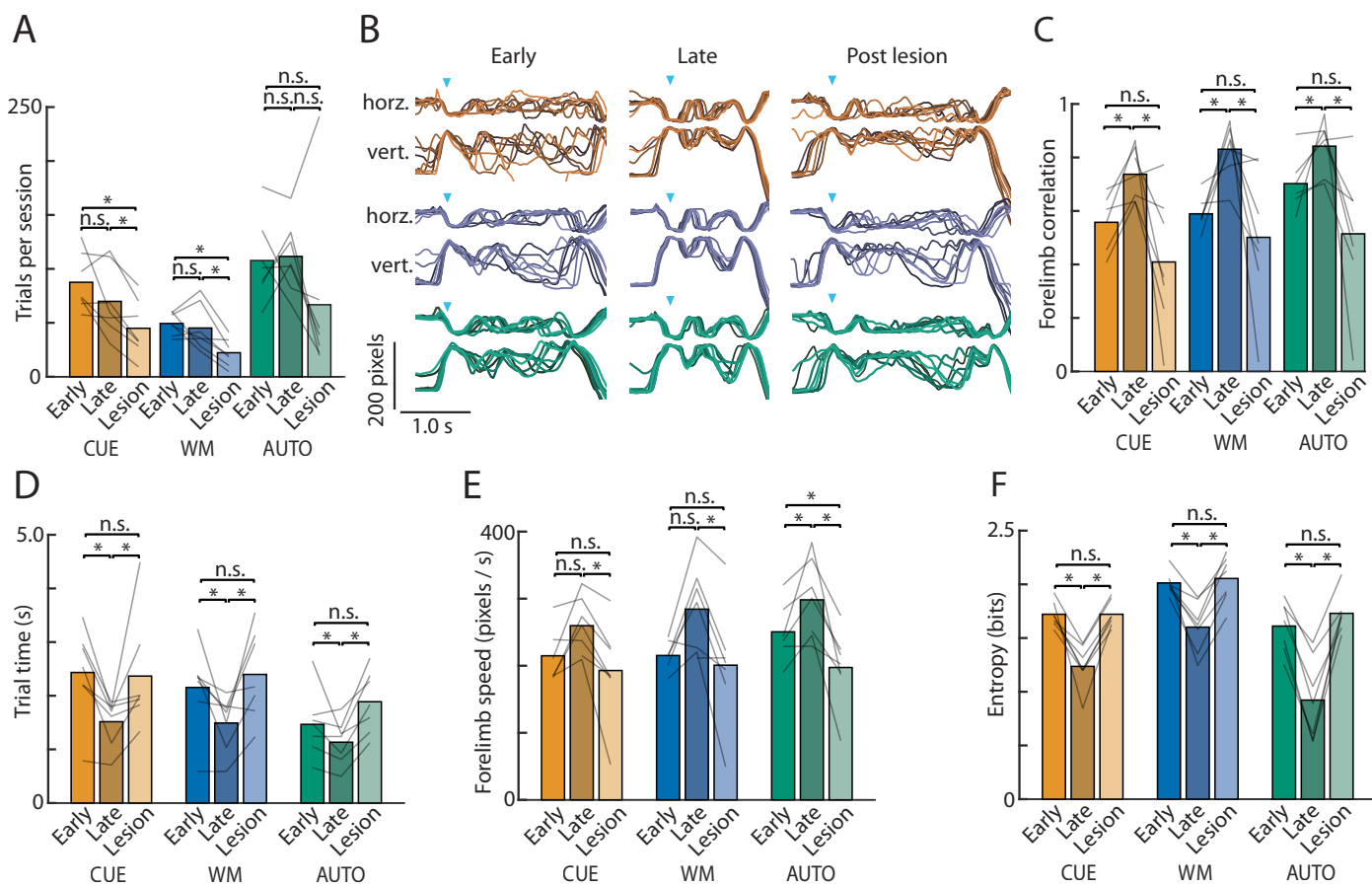
**Extended Data Fig. 6 | DLS encodes 3d nose and forelimb kinematic trajectories.** **a.** Views from our three cameras (right, left, and top) are shown, along with a set of static features in the box that were used to calibrate multiple views to the world for triangulation<sup>151</sup>. To triangulate the forelimb, the left and right view were calibrated using the blue points. To triangulate the nose, the top and either left or right view were calibrated using the yellow or red points. Some points are shared across calibrations. **b.** An example trajectory of the forelimb (left) and nose (right) plotted in 3 dimensions, during performance of the sequence C->R->C. Forelimb coordinates are relative to the top-left blue point in

A, and nose coordinates are relative to the top-left yellow point in A. **c–e.** Decoding analysis, performed the same as in Fig. 4f–h. **c.** Schematic of the decoding analysis. A feed-forward neural network is trained to predict the velocity components (x, y, and z) of the nose and forelimb in 3 dimensions. **d.** (Top) Heatmap of normalized forelimb (left) and nose (right) velocities in each dimension, observed in an example flexible session. (Bottom) Heatmap of the predicted forelimb and nose velocities output by our model. **e.** Decoding performance, measured in pseudo-R<sup>2</sup> of the model on a held-out set of test trials (see Methods). Dots indicate model performance on individual rats, and bar is average over rats ( $n = 4$ ).



**Extended Data Fig. 7 | Performance on 3-lever task is unaffected by a 7-day mock break.** **a-f.** Performance metrics before and after the mock break, in expert animals. Gray lines represent individual rats ( $n = 7$ ), bars are averages across rats. **a.** Normalized success rate, **b.** Trial time, **c.** Variance in the trial time,

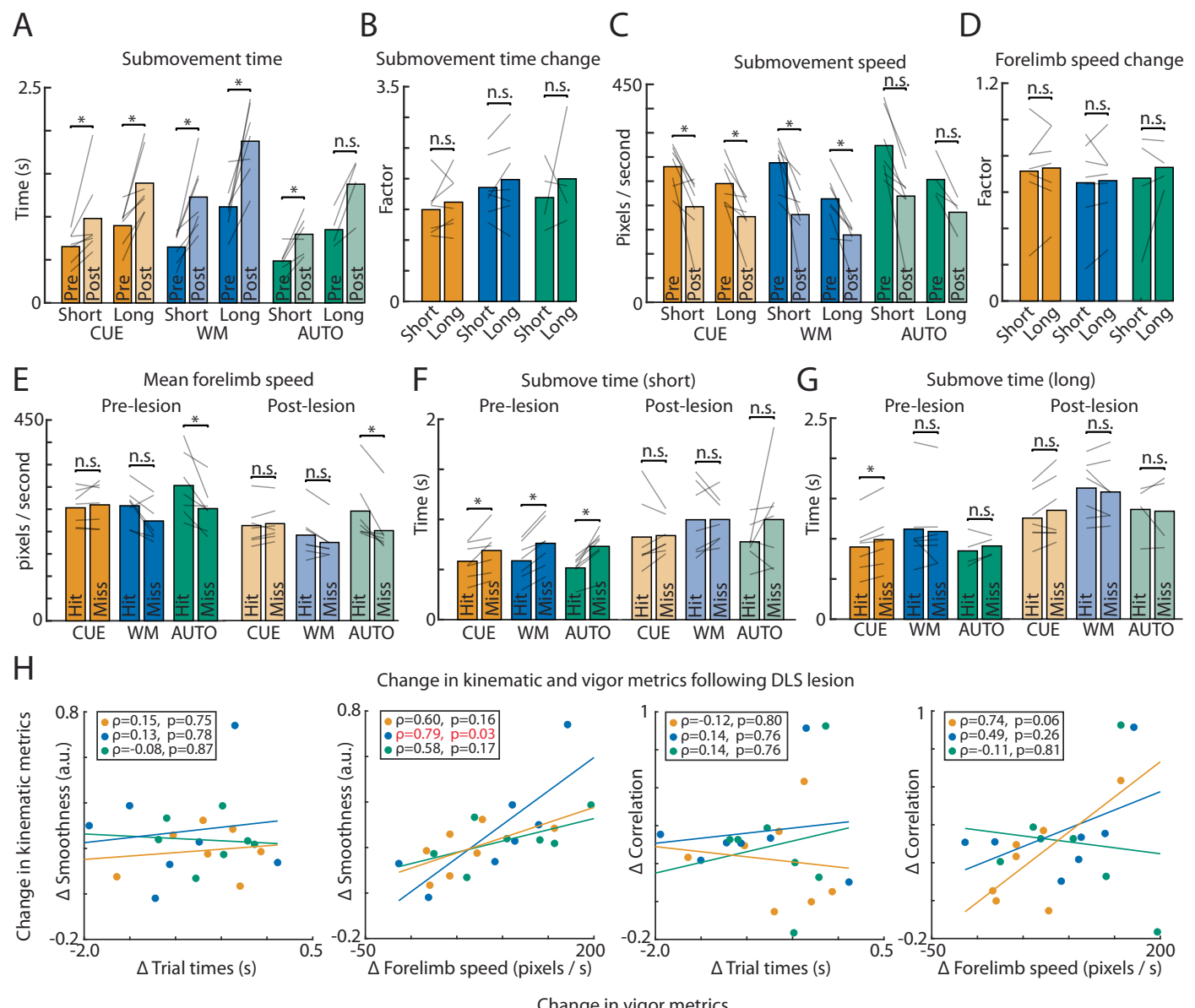
**d.** Entropy, or randomness, of errors, **e.** Average speed during the trial, **f.** Average trial-to-trial correlation. \* $P < 0.05$  Wilcoxon two-sided signed rank test. Orange – CUE, Blue – WM, Green – AUTO.



**Extended Data Fig. 8 | Post-lesion kinematics are more similar to early in learning.** **a.** Trials presses per session for both CUE, WM, and AUTO sequences decrease on average following the lesion. The average number of trials per session was not significantly different between the flexible (CUE and WM) and automatic (AUTO) session types before ( $p = 0.9375$ ) or after ( $p = 0.8125$ , Wilcoxon sign-rank test) the lesion ( $n = 7$  rats). **b.** Forelimb kinematics from 8 example trials of the same sequence, from one rat, sampled early in learning, late in learning, and following the bilateral DLS lesion (also see Fig. 1e, Fig. 5e, and see Methods for timing). **c.** Average trial-to-trial correlation for forelimb trajectories of the active

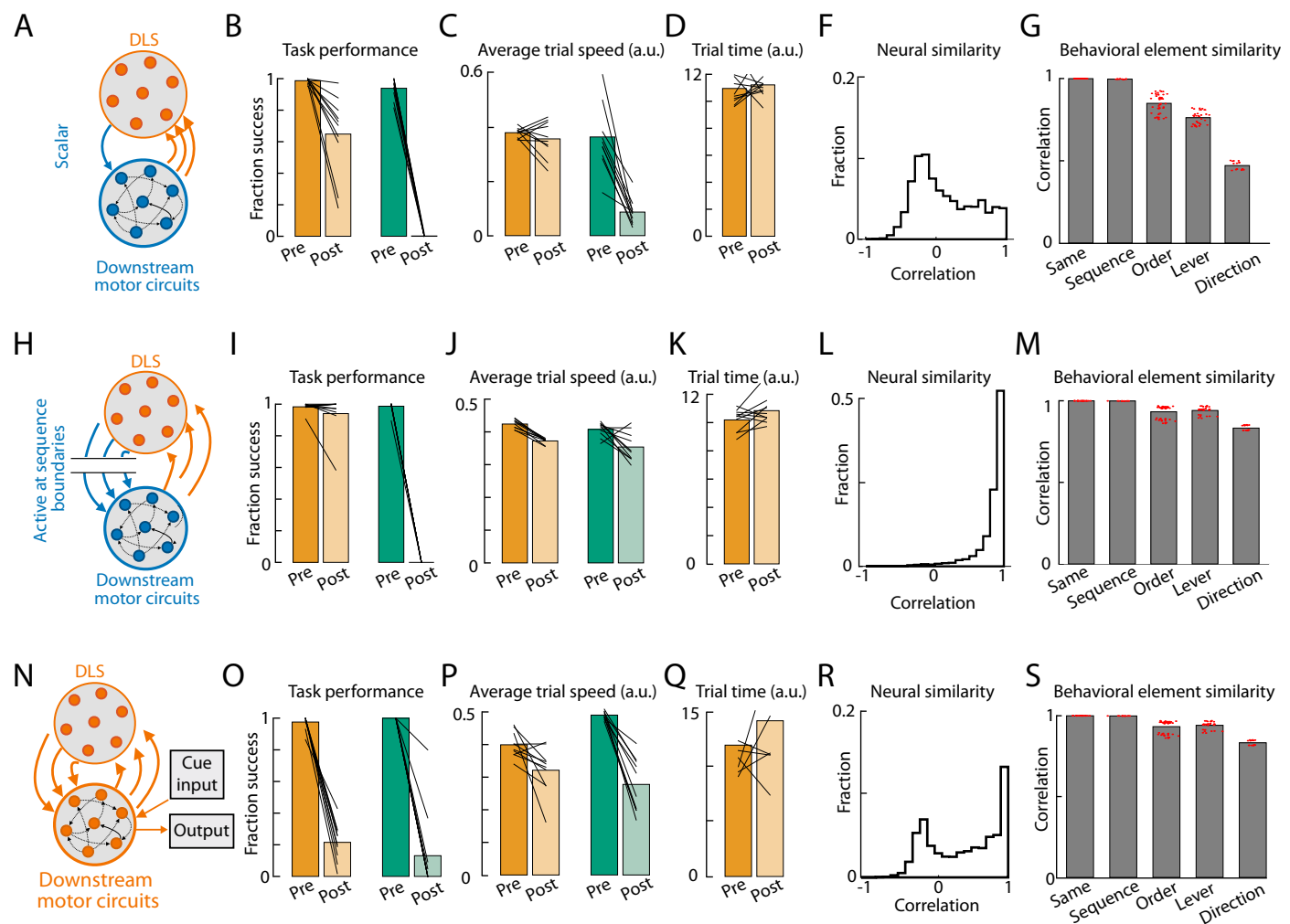
paw (both horizontal (x) and vertical (y)) from early in training, compared to late (pre-lesion), and post-lesion, for all task conditions (orange=CUE, blue=WM, green=AUTO). Gray lines are average within rats ( $n = 7$  late and lesion,  $n = 6$  early, 1 rat was not recorded early in learning) and bars represent average across rats.

**d.** Trial time from 1st to 3rd lever press early, late (or pre-lesion), and post-lesion ( $n = 7$  rats). **e.** Average forelimb speed during the trial ( $n = 7$  rats late and lesion,  $n = 6$  rats early). **f.** Variability in errors, measured through the Shannon entropy of the error distribution (see Methods,  $n = 7$  rats). \* $P < 0.05$ , Wilcoxon two-sided sign-rank test.



**Extended Data Fig. 9 | The effect of DLS lesion on different types of orientating movements, and on vigor and kinematics.** **a–d.** The effect of DLS lesions on short (for example, L > C) and long (for example, L > R) orientation movements. **a.** Plotted is the average inter-lever interval, split by short and long orientation movements, before (darker shade) and after (lighter shade) the lesion, for each task condition (CUE – orange, WM – blue, AUTO – green). Note that only 4 of 7 rats had long orientation movements in their prescribed AUTO sequence. In all plots, lines represent averages within individual rats, and bars are grand averages over all rats ( $n = 7$  except where noted). **b.** The factor increase in trial time (post lesion time/pre lesion time) is similar for short and long movements ( $n = 7$  rats, or  $n = 4$  for AUTO). **c–d.** Similar to A-B, but for the average forelimb speed during the orientation movements (submovements). **e–g.** The effect of DLS lesion on the vigor of successful and unsuccessful orienting movements. **e.** Average forelimb speed of successful and unsuccessful trials, for

CUE (orange), WM (blue), and AUTO (green) trial types, plotted pre (darker bars) and post (lighter bars) DLS lesion ( $n = 7$  rats). **f–g.** Average inter-lever interval (submovement time) for actions performed in successful (Hit) and unsuccessful (Miss) trials ( $n = 7$  rats). **f.** For short (for example, L > C) submovements, and **g.** long (for example, L > R) submovements. Only 4 of 7 rats had a long orientation movement in the AUTO sequence. **h.** The effect of DLS lesion on vigor compared to the effect of DLS lesion on kinematics (from Fig. 6e–i). Plotted is the change in vigor (that is, trial time or forelimb speed, plotted on the x-axis) against the change in kinematics (that is, movement smoothness or forelimb correlation, plotted on the y-axis). Each graph is a different kinematic vs. vigor metric comparison, and each dot indicates one rat, and the color indicates the task condition. Correlations between vigor and kinematics are calculated within each task condition for all rats (plot insets). \* $p < 0.05$ , Wilcoxon two-sided sign rank test.



**Extended Data Fig. 10 | Alternative network models fail to reproduce experimental results.** **a–g:** A neural network model with scalar DLS outputs fails to learn task-invariant DLS activity. **a:** Schematic illustrating architecture of a model variant in which DLS outputs to downstream motor circuits are constrained to be scalar-valued. **b–g:** Replication of analyses in Fig. 8d, f–i, for this model variant ( $n = 10$  runs). The neural representations are much less similar across task conditions than in the original model (panels E and F here versus Fig. 8d, f). **h–m:** A neural network model with action selection signals fails to learn strong kinematic representations. **h:** Schematic illustrating architecture of a model variant in which DLS outputs to downstream motor circuits are

suppressed except at trial initiation and transitions between lever presses. **i–m:** Replication of analyses in Fig. 8d, f–i, for this model variant ( $n = 10$  runs). The neural representations show much less egocentricity than in the original model (panel M here vs. Figure 8f). **n–s:** A neural network model without pre-trained circuits is not robust to DLS lesions in the flexible task. **n:** Schematic illustrating architecture of a model variant in which the entire model is trained on the cued and automatic tasks from scratch, rather than using the strategy of pretraining downstream motor circuits on cued trials first. **o–s:** Replication of analyses in Fig. 8d, f–i, for this model variant ( $n = 10$  runs). The resilience of flexible task performance seen in the original model is lost (panel O here versus Fig. 8g).

## Reporting Summary

Nature Portfolio wishes to improve the reproducibility of the work that we publish. This form provides structure for consistency and transparency in reporting. For further information on Nature Portfolio policies, see our [Editorial Policies](#) and the [Editorial Policy Checklist](#).

### Statistics

For all statistical analyses, confirm that the following items are present in the figure legend, table legend, main text, or Methods section.

n/a Confirmed

- The exact sample size ( $n$ ) for each experimental group/condition, given as a discrete number and unit of measurement
- A statement on whether measurements were taken from distinct samples or whether the same sample was measured repeatedly
- The statistical test(s) used AND whether they are one- or two-sided  
*Only common tests should be described solely by name; describe more complex techniques in the Methods section.*
- A description of all covariates tested
- A description of any assumptions or corrections, such as tests of normality and adjustment for multiple comparisons
- A full description of the statistical parameters including central tendency (e.g. means) or other basic estimates (e.g. regression coefficient) AND variation (e.g. standard deviation) or associated estimates of uncertainty (e.g. confidence intervals)
- For null hypothesis testing, the test statistic (e.g.  $F$ ,  $t$ ,  $r$ ) with confidence intervals, effect sizes, degrees of freedom and  $P$  value noted  
*Give P values as exact values whenever suitable.*
- For Bayesian analysis, information on the choice of priors and Markov chain Monte Carlo settings
- For hierarchical and complex designs, identification of the appropriate level for tests and full reporting of outcomes
- Estimates of effect sizes (e.g. Cohen's  $d$ , Pearson's  $r$ ), indicating how they were calculated

*Our web collection on [statistics for biologists](#) contains articles on many of the points above.*

### Software and code

Policy information about [availability of computer code](#)

Data collection	Behavioral data was acquired using custom software, based on a design in Poddar et al. 2013, and implemented with Raspberry Pi 3 and Teensy 3.6 microcontrollers. Electrophysiology data was acquired using custom software described in Dhawale et al. 2017 ( <a href="https://github.com/Olveczky-Lab/FAST-ChainViewer">https://github.com/Olveczky-Lab/FAST-ChainViewer</a> ).
Data analysis	Data analysis was performed using custom code written in Matlab 2021b (Mathworks). Code is available at <a href="https://github.com/kmizes/DLS-paper">https://github.com/kmizes/DLS-paper</a> . For kinematic tracking, the DeeperCut 1.0 implementation in tensorflow (Insafutdinov et al. 2016) was used ( <a href="https://github.com/eldar/pose-tensorflow">https://github.com/eldar/pose-tensorflow</a> ), together with custom code written in Matlab 2021b. Models were built and run using Pytorch version 1.12.1 in Python version 3.7.3.

For manuscripts utilizing custom algorithms or software that are central to the research but not yet described in published literature, software must be made available to editors and reviewers. We strongly encourage code deposition in a community repository (e.g. GitHub). See the Nature Portfolio [guidelines for submitting code & software](#) for further information.

## Data

Policy information about [availability of data](#)

All manuscripts must include a [data availability statement](#). This statement should provide the following information, where applicable:

- Accession codes, unique identifiers, or web links for publicly available datasets
- A description of any restrictions on data availability
- For clinical datasets or third party data, please ensure that the statement adheres to our [policy](#)

The generated datasets are available at <https://github.com/kmizes/DLS-paper>. Details and download of data used to pretrain DeeperCut can be found at: <https://pose.mpi-inf.mpg.de/#related>.

## Human research participants

Policy information about [studies involving human research participants and Sex and Gender in Research](#).

Reporting on sex and gender

N/A

Population characteristics

N/A

Recruitment

N/A

Ethics oversight

N/A

Note that full information on the approval of the study protocol must also be provided in the manuscript.

## Field-specific reporting

Please select the one below that is the best fit for your research. If you are not sure, read the appropriate sections before making your selection.

Life sciences

Behavioural & social sciences

Ecological, evolutionary & environmental sciences

For a reference copy of the document with all sections, see [nature.com/documents/nr-reporting-summary-flat.pdf](https://nature.com/documents/nr-reporting-summary-flat.pdf)

## Life sciences study design

All studies must disclose on these points even when the disclosure is negative.

Sample size

No statistical methods were used to pre-determine the number of subjects in our study, but our sample sizes are similar to those reported in previous publications (Jin et al., 2014, Rueda-Orozco and Robbe, 2015, Dhawale and Wolff et al., 2021)

Data exclusions

Animals were excluded from experiments post-hoc if the lesions were found to be small or outside of the intended target area (n=4 animals were excluded based on these criteria).

Replication

All lesions and recordings were performed in multiple animals per group (n>=4) and yielded consistent, reproducible findings within each cohort.

Randomization

Animals were randomly assigned to experimental groups.

Blinding

Experimenters were not blinded to group allocation for neural and behavioral data analysis. Since comparisons were made within groups and not across, no blinding was necessary.

## Reporting for specific materials, systems and methods

We require information from authors about some types of materials, experimental systems and methods used in many studies. Here, indicate whether each material, system or method listed is relevant to your study. If you are not sure if a list item applies to your research, read the appropriate section before selecting a response.

## Materials & experimental systems

n/a	Involved in the study
<input checked="" type="checkbox"/>	Antibodies
<input checked="" type="checkbox"/>	Eukaryotic cell lines
<input checked="" type="checkbox"/>	Palaeontology and archaeology
<input type="checkbox"/>	Animals and other organisms
<input checked="" type="checkbox"/>	Clinical data
<input checked="" type="checkbox"/>	Dual use research of concern

## Methods

n/a	Involved in the study
<input checked="" type="checkbox"/>	ChIP-seq
<input checked="" type="checkbox"/>	Flow cytometry
<input checked="" type="checkbox"/>	MRI-based neuroimaging

## Animals and other research organisms

Policy information about [studies involving animals](#); [ARRIVE guidelines](#) recommended for reporting animal research, and [Sex and Gender in Research](#)

### Laboratory animals

Experimental subjects were female Long Evans rats (RRID: RGD\_2308852) 3-10 months old at the start of training

### Wild animals

The study did not involve wild animals.

### Reporting on sex

Only female Long Evans rats were used in this study.

### Field-collected samples

The study did not contain samples collected from the field.

### Ethics oversight

The care and experimental manipulation of all animals were reviewed and approved by the Harvard Institutional Animal Care and Use Committee

Note that full information on the approval of the study protocol must also be provided in the manuscript.